CROATICA CHEMICA ACTA
CCACAA, ISSN-0011-1643, ISSN-1334-417X

Croat. Chem. Acta **82** (2) (2009) 363–386
CCA-3327

Authors' Review

Silicate Minerals from Macedonia. Complementary Use of Vibrational Spectroscopy and X-ray Powder Diffraction for Identification and Detection Purposes*

Gligor Jovanovski,[a,b,] Petre Makreski,[a] Branko Kaitner,[c] and Blažo Boev[d]**

[a]*Institute of Chemistry, Faculty of Science, SS. Cyril and Methodius University, P.O. Box 162, MK-1001 Skopje, Republic of Macedonia*
[b]*Macedonian Academy of Sciences and Arts, P.O. Box 428, MK-1001 Skopje, Republic of Macedonia*
[c]*Department of Chemistry, Faculty of Science, University of Zagreb, Horvatovac 102a, 10000 Zagreb, Croatia*
[d]*Faculty of Mining, Geology and Polytechnic, Goce Delčev University, Krste Misirkov bb, P.O. Box 201, MK-2000 Štip, Republic of Macedonia*

RECEIVED MARCH 25, 2008; REVISED SEPTEMBER 30, 2008; ACCEPTED OCTOBER 6, 2008

Abstract. Review of the results of complementary use of vibrational spectroscopy (infrared and Raman) and X-ray powder diffraction in the process of detection and identification of the silicate minerals from the Republic of Macedonia is presented.

Keywords: silicate minerals identification, powder X-ray diffraction, vibrational spectroscopy

INTRODUCTION

Republic of Macedonia lies in the Alpine–Balkan–Carpathian–Dinaride collision belt being rather rich in minerals. A large number of carbonate, sulfate, sulfide, oxide, silicate and other types of ore deposits are present in the R. Macedonia. For instance, there is a unique ore deposit at Alšar (near the Macedonian-Greek border) where 44 mineral species have been identified up to now. In spite of the plethora scientific papers regarding the spectroscopic and structural characterization and identification of the minerals from the R. Macedonia published so far, the total number of minerals present in Macedonia is not yet fully established. There are a few incomplete mineral collections, but no comprehensive literature data in which minerals from R. Macedonia would be systematized and characterized are available. In order to prepare the *Atlas of Minerals from R. Macedonia*, the systematic process of collection, separation, identification and systematizaton as well as spectroscopic and structural characterization of minerals originating from the R. Macedonia is undertaken. Silicate minerals are considerable part of the complete mineral wealth of the R. Macedonia.

The minerals are studied mainly by Fourier transform infrared (FT-IR) and Raman vibrational spectroscopy and by X-ray powder diffraction (XRPD).[1–30] In order to determine the presence and content of trace elements in the minerals atomic absorption spectrometry and inductively coupled plasma-atomic emission spectrometry are also used and analytical methods for discrimination between some mineral species are developed.[31–63] Various instrumental techniques and procedures for mineral detection, identification, discrimination and quantitative determination have been developed during the last few decades. The most frequently used among them are X-ray diffraction,[64–66] infrared[65,67,68] and Raman[68–70] vibrational spectroscopy, thermal analysis[71] and optical diffuse reflectance[72] (only a selection of the relevant references is given above).

Here, a review of the results of the complementary use of vibrational spectroscopy (IR and Raman) and XRPD in the process of identification and detection of the neso-, soro-, and inosilicate minerals from R. Macedonia is presented. The identification is based on the comparison of the results of our study with the corresponding literature data for the analogous mineral species originating from other localities in the world. In

* Dedicated to Professor Emeritus Drago Grdenić, Fellow of the Croatian Academy of Sciences and Arts, on the occasion of his 90th birthday.

** Author to whom correspondence should be addressed. (E-mail: gligor@iunona.pmf.ukim.edu.mk)

general, the comparison of the data is often accompanied by difficulties, the most important among them being related to: the instrument resolution; the temperature at which the experiment was performed; the sample preparation, particle size and shape; the studied vibrational spectral region and/or the 2 Θ region of the registered X-ray powder patterns; the specimen quantity used in the experiment; the locality where the specimen was collected from, *etc*.

EXPERIMENTAL

The studied minerals were collected from various localities (Figure 1). After that, single grains were carefully picked up under a microscope and then powdered.

Philips Analytical X-ray diffractometer PW 3710 was used for X-ray powder diffraction (step 0.01°, time per step 2.5 s). Generator with 50 kV and current 30 mA employed as a source for Cu$K\alpha$ radiation. The unit cell parameters were calculated from their X-ray diffraction patterns using CRYSFIRE software[73]. The obtained values were refined using CHECKCELL[74] (a modified version of CELREF for analysing the solutions given by the CRYSFIRE).

The mid-IR spectra of the studied samples were recorded on Perkin-Elmer FT-IR system 2000 interferometer using the KBr pellet method.

The Raman spectra were recorded on four instruments: computerized Dilor Z24 triple dispersive monochromator with Coherent Innova 400 argon ion laser operating at 514.5 nm for excitation, micro-Raman multichannel spectrometer – Horiba Jobin Yvon LabRam Infinity ($f \times 100$) operating at 532 nm laser line obtained from a Nd-YAG frequency-double laser; Bruker FT Raman model 106/S connected to FT-IR interferometer Equinox 55 with 1064 nm line of Nd-YAG frequency laser; Renishaw micro-Raman 1000 spectrometer equipped with a Peltier cooled CCD camera and Leica microscope ($f \times 50$), the Raman effect being excited using the 514 nm line of an air cooled Ar^+ laser by Melles Griot.

The measurements were carried at a room temperature (RT) and GRAMS/32 software[75] package was applied for the spectral manipulations.

Chemical composition of the minerals was analyzed by electron microprobe analyzer (EMS) CAMECA. The presented mineral analyses represent the average values obtained from three different points.

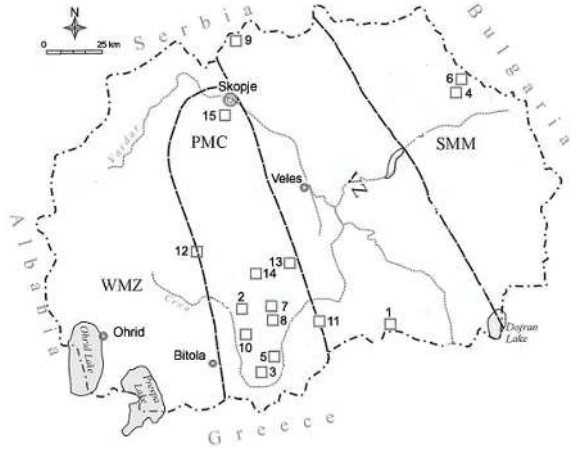

Figure 1. The silicate localities in the Republic of Macedonia with the studied minerals: 1) Ržanovo (olivine), 2) Alinci (arfvedsonite), 3) Čanište (epidote), 4) Petrova Reka (rhodonite), 5) Dunje (titanite), 6) Sasa (hemimorphite, ilvaite, hedenbergite, ferrojohansennite, bustamite), 7) Štavica (staurolite), 8) Čumovo (kyanite), 9) Lojane (spessartine), 10) Staro Bonče (almandine), 11) Vrpsko (carpholite), 12) Košino (actinolite-tremolite), 13) Kozjak (zircon), 14) Pelagon (hornblende), 15) Vodno (glaucophane).

GEOLOGICAL SETTING OF THE R. MACEDONIA

Four geotectonic regions are present in the territory of the R. Macedonia: Serbian-Macedonian Massive (SMM); Vardar Zone (VZ); Pelagonian Metamorphic Complex (PMC); West-Macedonian zone (WMZ)[76] (see Figure 1).

In addition to other mineral types, the geologic constitution of the R. Macedonia is characterized by the presence of a large number of silicate minerals in all mentioned geotectonic units, the most prominent one being the PMC. More details related to the geological setting as well as to the silicate deposits and occurrences in the R. Macedonia are given in Ref. 17.

CLASSIFICATION OF SILICATES

About 4000 minerals have been identified and named by now.[77–80] Approximately 30 % of them belong to the silicate class which is the most abundant group of minerals in the Earth's crust. Most of the silicate minerals are drab and commonplace, while a few of them are used as precious gemstones. However, they are very important economic resources being used as industrial materials. The silicate minerals also make agriculture possible as a most dominant component of soil (mostly quartz and clays). The elementary building unit of the silicate minerals is the SiO_4 tetrahedron having a net –4 charge. The interlinking of the SiO_4 tetrahedra results in formation of various polymers. The structural classification of the silicate minerals is in fact based on the

extent of sharing of oxygen anions between the adjacent tetrahedra. It makes the silicates the largest and the most complicated class of minerals.

RESULTS AND DISCUSSION

Determination of the Chemical Composition of the Minerals

The chemical analysis of the minerals (Table 1) was conduced in order to determine the minerals composition. It was shown that it is especially important for the minerals that form solid solutions because according to the chemical composition one could evaluate whether the studied sample represents the endmember of the mineral series or its composition ranges between the endmembers. It is also very important from the viewpoint that sometimes even small compositional differences within the minerals forming one series could manifest smaller or even larger discrepancies within their vibrational spectra. The situation is even more significant when the view of the vibrational spectra could serve as an indicator to predict whether the sample represents endmember or it is only a part of that series. Here it could be mentioned, for example, that the chemical composition of the several studied minerals was found to be closer to ferrojohannsenite, magnesioarfvedsonite, ferroglaucophane and ferrohornblende, than to johannsenite, arfvedsonite, glaucophane and magnesiohornblende, respectively[80] (Table 1). Therefore, the chemical formula for each studied mineral is written according to determined chemical composition (Table 1).

Nesosilicates (Orthosilicates)

In order to be identified and characterized, the vibrational spectra and powder X-ray diffraction patterns of seven common nesosilicate minerals: almandine, $Fe_3Al_2(SiO_4)_3$; spessartine, $Mn_3Al_2(SiO_4)_3$; zircon, $ZrSiO_4$; titanite, $CaTiOSiO_4$; olivine, $(Mg,Fe)_2SiO_4$; kyanite, Al_2OSiO_4 and staurolite, $Fe_2Al_9O_6(SiO_4)_4(OH)_2$ [17,21,24,29] were studied.

Numerous investigations have been undertaken to elucidate the IR spectra of almandine,[81–85] spessartine,[81,83–85] zircon,[81,86–88] titanite,[81] olivine,[81,83,89,90] kyanite,[81,91,92] and staurolite.[81,93] In addition, Raman spectra of almandine,[84,85,94–97] spessartine,[85,94–96] zircon,[94,97] titanite,[94,98] olivine[94,99] and kyanite[100] were additionally used for mineral characterization. The Raman spectrum of staurolite, to the best of our knowledge, has not been published in the literature.

The details of the complementary use of vibrational spectroscopy and powder X-ray diffraction for identification and detection of nesosilicates (orthosilicates) from R. Macedonia are summarized in review.[24] Here, only some improved results obtained in the meantime for almandine, spessartine and olivine will be presented.

Almandine, $(Fe,Mg,Ca)_3Al_2(SiO_4)_3$, from Staro Bonče and Spessartine, $(Mn,Ca,Mg,Fe)_3Al_2(SiO_4)_3$, from Lojane

The dispersive (514 nm) and FT-Raman (1064 nm) spectra of almandine (Figure 2 in Ref. 21) are, to some extent, similar, but show some significant differences (Table 4 in Ref. 21) suggesting that one should be careful during their use for identifycation purposes as well as for spectra–structure correlations.[21] In fact, all bands observed in the dispersive Raman spectrum are present in the FT-counterpart, where two additional strong bands at 607 and 446 cm^{-1} were registered. Since, the dispersive Raman spectrum showed a closer similarity with the corresponding spectrum of the isomorphous spessartine analogue (Figure 23 in Ref. 24), it was presumed that more likely some structural changes appear during the recording of the almandine FT-Raman spectrum.[21,24] Later it was shown[29] that the strong bands in the FT-Raman spectrum of almandine (at 607 and 446 cm^{-1}) are fluorescence bands that appear from the traces of rare earth impurities in the sample (Figures 2 and 3). Therefore, the use of dispersive Raman instruments are more convenient for mineral strudies but when emplying the FT-Raman technique it is more than reccomendable to extend the spectral range in the Anti-Stokes side.

The identification of the almandine and spessartine mineral samples was confirmed by the study of

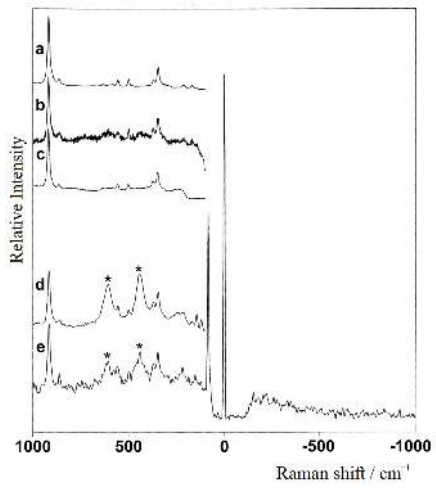

Figure 2. Dispersive Raman spectra of almandine (a, b, c) obtained with 532, 488 and 514.5 nm excitation line, respectively. FT-Raman spectra of almandine in Stokes (d) and in both Stokes and Anti-Stokes side (e) obtained with 1064 nm line. The fluorescence bands at 446 and 607 cm^{-1} in the FT-Raman spectra are denoted by asterisk.

Table 1. The element content (in %) obtained by electron microprobe analysis. The calculated content according to the empirical formula[80] is underlined

Mineral name	Ideal chemical formula (above) and Empirical formula (below)[80]	Chemical formula derived from chemical composition	Na_2O	K_2O	CaO	MgO	MnO	NiO	ZnO	FeO	Fe_2O_3	Al_2O_3	SiO_2	TiO_2
Almandine	$Fe_3Al_2(SiO_4)_3$ $Fe^{2+}_3Al_2(SiO_4)_3$	$(Fe,Mg,Ca)_3Al_2(SiO_4)_3$			5.10	7.23	0.04			30.20		21.33	35.96	
										43.30		20.48	36.21	
Spessartine	$Mn_3Al_2(SiO_4)_3$ $Mn^{2+}_3Al_2(SiO_4)_3$	$(Mn,Ca,Mg,Fe)_3Al_2(SiO_4)_3$			5.85	4.46	29.92			2.46		20.68	36.49	
							42.99					20.60	36.41	
Olivine	$(Mg,Fe)_2SiO_4$ $Mg_{1.6}Fe^{2+}_{0.4}(SiO_4)$	$(Mg,Fe)_2SiO_4$				50.82	0.06	0.32		7.70			40.77	
						42.06				18.75			39.19	
Epidote	$Ca_2(Fe,Al)_3(SiO_4)_3(OH)$ $Ca_2Fe^{3+}_{2.25}Al_{0.75}(SiO_4)_3(OH)$	$Ca_2Al_2(Fe,Al)(SiO_4)_3(OH)$			24.09		0.24				11.65	25.64	37.65	0.09
					21.60						34.60	7.36	34.71	
Hemimorphite	$Zn_4Si_2O_7(OH)_2{\cdot}H_2O$ $Zn_4Si_2O_7(OH)_2{\cdot}H_2O$	$Zn_4Si_2O_7(OH)_2{\cdot}H_2O$							66.77				25.14	
									67.58				24.94	
Ilvaite	$CaFe_2FeSi_2O_7O(OH)$ $CaFe^{2+}_3(SiO_4)_2(OH)$	$CaFe_2FeSi_2O_7O(OH)$			13.94					48.16			29.95	
					13.72					52.72			29.40	
Johannsenite	$CaMnSi_2O_6$ $CaMn^{2+}(Si_2O_6)$	$Ca(Fe,Mn)Si_2O_6$			22.17		3.66			23.84			49.82	
					22.69		28.7						48.62	
Hedenbergite	$CaFeSi_2O_6$ $CaFe^{2+}Si_2O_6$	$(Ca,Mg)(Fe,Mn)Si_2O_6$			19.14	1.61	11.06			17.12		2.18	48.26	
					22.60					28.96			48.44	
Rhodonite	$(Mn,Fe,Mg,Ca)SiO_3$ $Mn^{2+}_{3.9}Fe^{2+}_{0.02}Mg_{0.02}Ca_{0.05}SiO_3$	$(Mn,Ca)SiO_3$			8.94		41.61			2.19		0.22	46.89	
					2.17	0.62	49.44			1.11			46.53	
Bustamite	$(Mn,Ca)_3Si_3O_9$ $Mn^{2+}_{2.25}Ca_{0.75}Si_3O_9$	$(Mn,Ca,Fe)_3Si_3O_9$			17.23		26.14			8.09		0.17	47.38	
					11.01		41.79						47.20	
Carpholite	$MnAl_2Si_2O_6(OH)_4$ $Mn^{2+}Al_2Si_2O_6(OH)_4$	$(Mn,Mg)Al_2Si_2O_6(OH)_4$			0.02	5.73	13.60			0.47		35.24	40.12	
							21.56					30.89	36.51	
Mg-arfvedsonite	$NaNa_2(Mg_4Fe)Si_8O_{22}(OH)_2$ $Na_3Mg_4Fe^{3+}(Si_8O_{22})(OH)_2$	$Na_2(Na,K)(Mg,Fe,Ca)_5Si_8O_{22}(OH)_2$	7.39	1.50	2.69	14.12	0.47				15.51	2.23	53.76	0.13
			11.16			19.36					9.59		57.72	
Fe-glaucophane	$Na_2(Fe_3Al_2)Si_8O_{22}(OH)_2$ $Na_2Fe^{2+}_3Al_2(Si_8O_{22})(OH)_2$	$Na_2(Mg,Fe)_3(Fe,Al)_2Si_8O_{22}(OH)_2$	6.49	0.05	0.77	4.86	0.24				26.02	7.13	52.47	0.03
			7.06								27.28	11.61	54.74	
Actinolite	$Ca_2(Mg,Fe)_5Si_8O_{22}(OH)_2$ $Ca_2Mg_5Si_8O_{22}(OH)_2Fe^{2+}_2$	$Ca_2(Mg,Fe)_5Si_8O_{22}(OH)_2$	0.62	0.08	11.43	21.16	0.21				4.33	1.61	58.20	0.01
					12.81	13.81					18.24		54.91	
Fe-hornblende	$Ca_2[Fe_4(Al,Fe)]Si_7AlO_{22}(OH)_2$ $Ca_2Fe^{2+}_4Al_{0.75}Fe^{3+}_{0.25}[Si_7AlO_{22}](OH)_2$	$(Na,K)_0Ca_2(Mg,Fe,Fe,Al)_5(Si,Al)_8C_{22}(OH)_2$	0.63	0.63	11.03	10.05	0.31				18.77	9.09	47.34	0.15
					11.84						35.81	9.42	44.40	

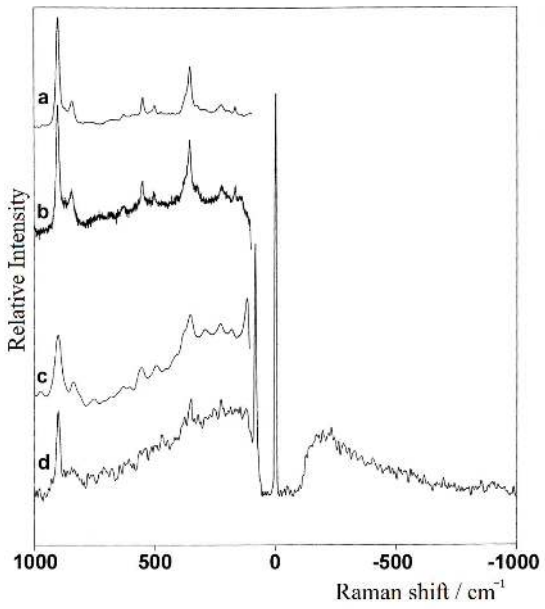

Figure 3. Dispersive Raman spectra of spessartine (a, b) obtained with 532 and 488 nm excitation line, respectively. FT-Raman spectra of spessartine in Stokes (c) and in both Stokes and Anti-Stokes side (d) obtained with 1064 nm line.

their XRPD patterns (Tables 24 and 25 in Ref. 24). The very good correlation between the obtained and the literature XRPD data for almandine (Table 2) and spessartine (Table 3) confirmed the authenticity of the studied samples.[21,24,29,101]

Olivine, $(Mg,Fe)_2SiO_4$, from Ržanovo

The term olivine, $(Mg,Fe)_2SiO_4$ represents solid solutions of the isomorphous forsterite, Mg_2SiO_4, and fayalite, Fe_2SiO_4. The criterion that all IR bands of the forsterite-fayalite series show a frequency shift of peak maxima to lower values with increasing iron content,[90] enabled to discriminate between them as well as to estimate the olivine composition from the IR spectra. Namely, the application of this criterion to the IR spectrum of the studied olivine showed that the band frequencies are much closer to the corresponding bands in the spectrum of forsterite, Mg_2SiO_4.[21,24] The presence of two strong bands (at 417 and 608 cm^{-1}) in the IR spectrum of forsterite, absent in the spectrum of fayalite (Table 10 in Ref. 21) may serve as a further aid to discriminate between the two end members of olivine series. An additional discriminating feature is the lack of bands below 450 cm^{-1} in the spectrum of fayalite that are present in the spectrum of forsterite.

The identification of the studied mineral as forsterite by IR spectroscopy was, at some extent, supported by the appearance of its low quality dispersive Raman spectrum (Figure 5b in Ref. 21). Later the higher quality corresponding spectrum was recorded (Figure 4b, Table 4) providing much better agreement with the literature data.[94,99] Additional similarities between the Raman spectrum of the studied sample and the corresponding spectrum of forsterite (rather than that of fayalite) were observed, as well.

The comparison of the literature X-ray powder diagrams of forsterite and fayalite,[101] on the one hand, and of the studied sample, on the other hand (Figure 30 in Ref. 24), as well as the registered complete agreement of the XRPD data of the studied olivine specimen from

Table 2. The most intensive maxima and the unit cell parameters derived from the X-ray powder diagram of the studied almandine

h	*k*	*l*	d_{obs}	d_{cal}	d_{diff}
4	0	0	1.4961	1.4949	0.0012
4	0	2	1.3503	1.3501	0.0002
2	2	4	1.2453	1.2448	0.0005
1	0	5	1.2022	1.2020	0.0002
5	1	2	1.1304	1.1305	–0.0001
3	2	5	1.0254	1.0259	–0.0005
4	4	4	0.9384	0.9385	–0.0001
6	0	4	0.9123	0.9121	0.0002
6	2	4	0.8891	0.8894	–0.0003

Unit Cell Par. (obs)	Unit Cell Par.[102]
a = 11.5140 Å	a = 11.531 Å
V = 1526.425 Å^3	V = 1533.2 Å^3
	Cubic (*Ia3d*); Z = 8

Table 3. The most intensive maxima and the unit cell parameters derived from the X-ray powder diagram of the studied spessartine

h	*k*	*l*	d_{obs}	d_{cal}	d_{diff}
0	0	4	1.5125	1.5131	–0.0006
4	0	2	1.3661	1.3662	–0.0001
4	2	2	1.2591	1.2593	–0.0002
1	3	4	1.2156	1.2158	–0.0002
5	1	2	1.1429	1.1432	–0.0003
6	1	1	1.0368	1.0367	0.0001
4	4	4	0.9476	0.9475	0.0001
6	0	4	0.9207	0.9206	–0.0001
2	4	6	0.8972	0.8973	–0.0001

Unit Cell Par. (obs)	Unit Cell Par.[103]
a = 11.666 Å	a = 11.612 Å
V = 1587.707 Å^3	V = 1565.7 Å^3
	Cubic (*Ia3d*); Z = 8

Ržanovo with the corresponding diagram of forsterite[101] (Table 34 in Ref. 24) undoubtedly proves that the chemical composition of the studied sample is much closer to forsterite endmember. The results obtained by IR and Raman vibrational spectroscopy as well as by XRPD were confirmed by the X-ray microprobe analysis (Table 5).

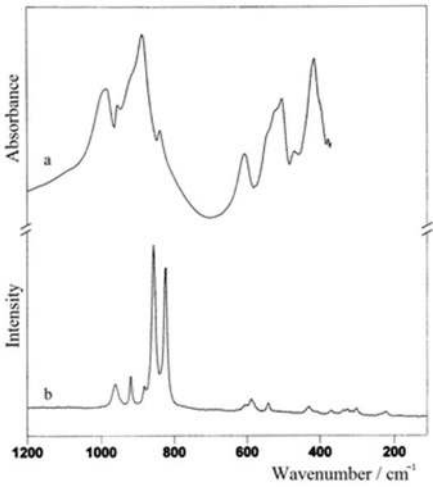

Figure 4. Infrared (a) and dispersive Raman spectra (b) of olivine from Ržanovo (variety forsterite).

Table 4. Frequences and intensities of the bands in the powder Raman spectrum of olivine (forsterite) compared with the corresponding literature data

This work[(a)]	Griffith[94] Mg_2SiO_4	Griffith[94] Fe_2SiO_4	Guyot *et al.*[99 (b)]	Assigment[(c)]
960 w	950	–	960	ν_3(Si–O–Si)
919 sh	–	–	920	
876 sh	–	–	–	
855 vs	860	–	855	ν_3(Si–O–Si)
823 vs	823	828	824	ν_1(Si–O–Si)
605 vw	602	608		ν_4(Si–O–Si)
588 w	–	–		
542 w	546	550		ν_4(Si–O–Si)
430 w	465	–		ν_4(Si–O–Si)
369 vw	380	380		ν_2(Si–O–Si)
336 vw	–	–		
326 vw	327	–		ν_2(Si–O–Si)
302 vw	–	–		
223 vw	–	–		

[(a)]Excitation with 532 nm
[(b)]Only stretching with SiO_4 modes are discussed
[(c)]According to Griffith[94]

Sorosilicates (Disilicates)

The IR and Raman spectroscopy as well as PXRD were used in order to identify and characterize collected sorosilicate minerals: epidote, $Ca_2Al_2(Fe,Al)(SiO_4)(Si_2O_7)O(OH)$, hemimorphite, $Zn_4(Si_2O_7)(OH)_2\cdot H_2O$ and ilvaite, $CaFe_2^{2+}Fe^{3+}(Si_2O_7)O(OH)$.

Several studies have been undertaken to observe the infrared spectra of epidote[81,105–107] and hemimorphite.[81,108–111] The IR spectrum of ilvaite (in the SiO_4 region) has been published, but not discussed.[81,108,112] The consideration of their Raman spectra has not provoked much attention. Namely, the corresponding spectrum of epidote has only been reported by Wang *et al.*[113] without presented band assignments. Furthermore, to the best of our knowledge, the Raman data for hemimorphite have not been published in the literature, although the corresponding spectra of this mineral type can be found on Internet.[114,115] The Raman spectrum of ilvaite has neither been found in the literature nor on Internet. The detailed analysis of the IR and Raman spectra of epidote, hemimorphite and ilvaite made by us is given in Ref. 27. Here, only some characteristic spectral and structural features will be pointed out.

Infrared Spectral Study

OH Region. The chemical composition of these minerals is not necessarily fixed, especially for epidote-clinozoisite mineral series: $Ca_2Al_2(Fe,Al)(SiO_4)(Si_2O_7)O(OH)$ - $Ca_2Al_2Al(SiO_4)(Si_2O_7)O(OH)$, where the content of Fe and Al could substantially vary. In this context, it was shown that the intensity and especially the frequency of the IR band in the ν(OH) region could serve as a tool for reliable estimation of the Fe and/or Al content in epidote.

The strength of O–H bond slightly differs when different cations are coordinated to the hydroxyl group. Thus, the implementation of simple harmonic model of different M^{3+}–O oscillators (M = Fe and/or Al in epidote) would result in frequency shifting of the band in the spectrum. According to Langer and Raith,[105] mono-

Table 5. The chemical composition and the unit cell parameters (in Å) of the studied olivine sample compared to the corresponding data for the samples with the chemical composition close to forsterite and fayalite end members

	Ideal Chemistry	Obtained Chemistry	*a*	*b*	*c*	*V*	Space Group	*Z*
This work		$(Mg_{1.68},Fe^{2+}_{0.32})SiO_4$	4.7633	10.2280	5.9909	291.87	*Pbnm*	4
Forsterite	Mg_2SiO_4	$(Mg_{1.82},Fe_{0.18})SiO_4$	4.7617	10.2255	5.9927	291.79	*Pbnm*	4
Fayalite	$Fe^{2+}_2SiO_4$	$(Fe^{2+}_{1.88},Mn_{0.12})SiO_4$	4.8177	10.477	6.0922	307.5	*Pbnm*	4

clinic epidotes with variable (Fe,Al) composition exhibit a single OH-band, the position of which is a linear function of the Fe content. With increasing of the Fe content from 0.00 (in clinozoisite, $Ca_2Al_2Al(SiO_4)(Si_2O_7)O(OH)$) to 0.89 (in Fe-rich epidote), the position of this band shifts from 3326 to 3365 cm^{-1}, respectively, allowing a reliable estimation of the Fe content. It seems that the effect of Fe substituting for Al at the non-OH coordinated M1 and especially M3 octahedral sites causes an increase in the bond strength at the O4 atom ($^{[M2]}Al–O10–H\cdots O4–^{[M1]}Al^{[M1]}Al^{[M3]}Fe$) (for Fe it is principally due to the difference in the electronegativity with respect to Al.[107] Since the maximum of the OH stretching vibration in our IR spectrum is observed at 3362 cm^{-1} (Figure 5a) (Table 2 in Ref. 27), it is more likely that the studied mineral sample could preliminary be contemplated as epidote.

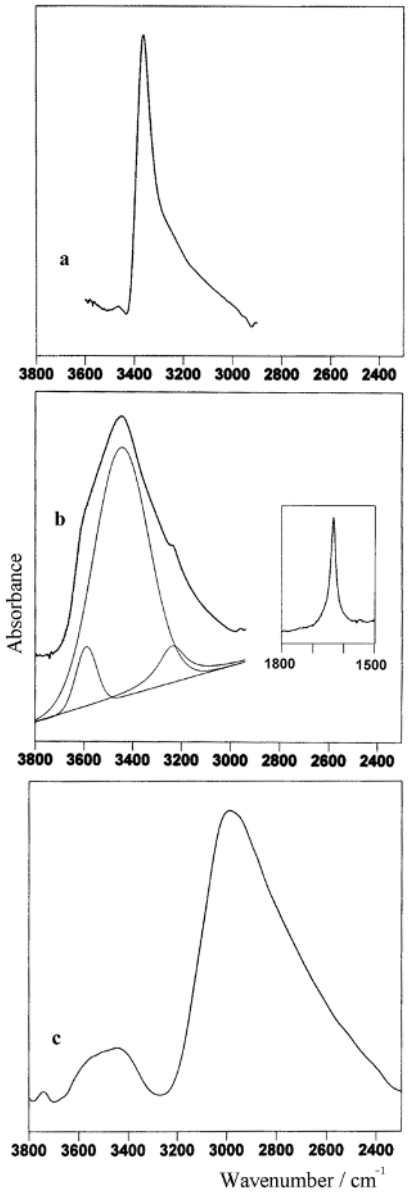

Figure 5. The stretching OH (and H_2O) region in the powder IR spectrum of epidote (a), hemimorphite (b) and ilvaite (c). The result of the curve-fitting is given below hemimorphite spectrum. The $\delta(H_2O)$ region (1800–1500 cm^{-1}) in hemimorphite is presented as well.

Very complex and strong band with the centroide around 3445 cm^{-1}, associated by two shoulders around 3610 cm^{-1} 3240 cm^{-1}, is main characteristic of the OH stretching region of the studied hemimorphite (Figure 5b). The band frequencies are in agreement with the published data for corresponding powdered sample (Table 3 in Ref. 27). Using the correlation diagrams of the O–H···O bond lengths *vs.* O–H stretching energies[116,117] (applied to hemimorphite structure[118]), the reported bands at 3439 cm^{-1} and 3616 cm^{-1} (along the polarized IR spectrum in *c*-direction) are prescribed to hydroxide and water stretching mode, respectively.[110] Having in mind that *v*(OH) vibrations in the OH bearing minerals are generally observed in the 3600–3400 cm^{-1} region, the band at 3610 cm^{-1} probably arise from FeOH strectchings, whereas the strongest band at 3445 cm^{-1} has OH and perhaps somewhat H_2O stretching mode character. Together with the registered band at 3240 cm^{-1} being an overtone of the bending H_2O mode around 1634 cm^{-1} (Table 3 in Ref. 27), the spectral view of the OH stretching region of powdered hemimorphite is somewhat clearer.

The intense band at 3000 cm^{-1} as well as the broad band ranging from 3600 to 3400 cm^{-1} observed in the ilvaite IR spectrum were attributed to the *v*(OH) vibrations.

Si_2O_7 Region. The IR spectrum of epidote represents rather complex pattern in the Si_2O_7 region (Figure 6a). The bands could be mainly divided in 2 regions: higher- (1150–750 cm^{-1}) and lower-frequency (750–370 cm^{-1}), but their origin has still not been completely elucidated.[106] Therefore an additional attempt to reveal some uncertainties concerning the IR assignments was made. The numeration of the bands (Figure 6a) is accepted from Langer and Raith,[105] whereas the complete assignment of the bands is given in Table 2 of Ref. 27.

It is worth mentioning that the absence of band 3, on one hand, and band 4, on the other, could strongly discriminate between epidote (Figure 6a) and isomorphous Fe-free clinozoisite mineral specie $Ca_2Al_2Al(SiO_4)(Si_2O_7)O(OH)$. Namely, it is found that bands 3 and 4 are due to the Si2–O8–M3 valence vibrations for the cases when the M3 sites are occupied by Al or Fe, respectively.[119] Obviously, the absence of Al cations in the epidote structure implies the absence of several additional IR bands (12, 14, 18 and 22), typical for the spectrum of clinozoisite.[116,119] It confirms that IR spec-

troscopy could differentiate between the two isomorphous minerals in both OH and SiO_4 (Si_2O_7) stretching (and bending) regions. Because of the complete dif-ference between epidote and clinozoisite spectra in 820–700 (bands 12–14) and 540–370 cm^{-1} (bands 20–28), the absorption in these regions is attributed to the M–O vibrations within the various octahedra of the two different structure types.[105]

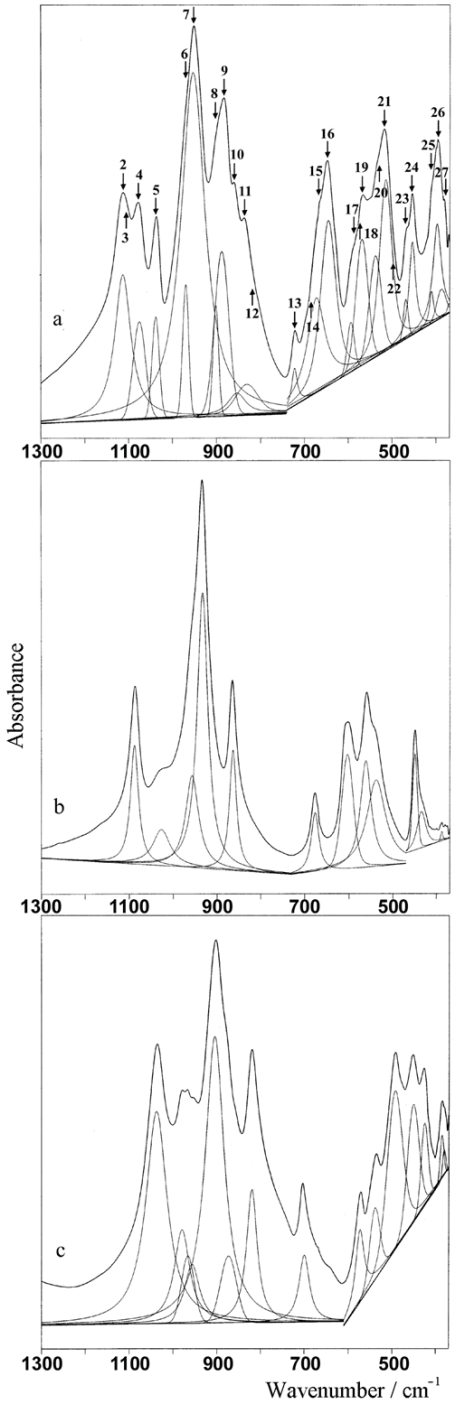

Figure 6. The powder IR spectrum of epidote (a), hemimorphite (b) and ilvaite (c) (1300–370 cm^{-1}). The result of the curve-fitting is given below each spectrum. The arrows and numbers above the epidote spectrum are attributed to the expected bands for this mineral, whereas those below indicate the bands typical for isomorphous clinozoisite mineral.

The number of the bands in the IR spectrum of hemimorphite (Figure 6b) in the higher-frequency region (1100–800 cm^{-1}) is smaller compared to the epidote counterpart. However, it is very similar with the published spectra of the corresponding mineral.[81,110,111] The presence of the bands in many sorosilicate spectra[120,121] at frequencies 1170–1080 cm^{-1} much above those from nesosilicates[21] implies that these bands could be assigned as ν_{as}(Si–O_b–Si) modes (O_b denotes bridging oxygens). Therefore, the origin of the band at 1088 cm^{-1} is not questionable and should be attributed to the mentioned Si–O vibration, despite the obviously wrong assignment as OH bendings proposed by Poulet and Mathieu[110] (see Table 3 in Ref. 27). The two weak bands below 450 cm^{-1} (at 435 and 388 cm^{-1}) are prescribed to the ν(Zn–O) modes. According to Brunel and Vierne[111] their weak intensity is related to the presence of the infinite Zn–O chains in the hemimorphite structure.

The infrared spectrum of ilvaite (Figure 6c) in the higher-frequency region (1300–700 cm^{-1}) shows similar pattern with the spectrum of hemimorphite (Figure 6b), whereas lower-frequency part (700–370 cm^{-1}) is much similar with the spectrum of epidote (Figure 6a). It could be explained by the fact that the main vibrational units responsible for the appearance of the bands in the higher-frequency part of the spectrum are Si_2O_7 blocks. The larger number of the bands in the epidote spectrum in this region is due to the presence of bands from the stretching vibrations of the SiO_4 tetrahedra also present in its structure. Since no interpretation of the ilvaite IR spectrum is found in the literature,[81,112] the assignments of the bands in its spectrum is mostly derived from the analogous hemimorphite and epidote spectral discussion (Table 4 in Ref. 27).

Shorter M1–O bond length (stronger force constant) compared to the M2–O bond length (M1, M2 = non-equivalent octahedral sites in ilvaite structure occupied by Fe^{2+} and Fe^{3+}, respectively) causes the appearance of the corresponding ν(M1–O) mode at about 70 cm^{-1} higher frequency compared to the ν(M2–O) mode (494 and 426 cm^{-1}, respectively) (Table 4 in Ref. 27).

Raman Spectral Study

Although the Raman spectrum of epidote has been published in the literature,[113] no band assignment is given. Its tentative interpretation was mainly based on the IR considerations. The highest-frequency bands in the 1100–800 cm^{-1} region were assigned as symmetric stretching Si–O_{nb} vibrations (from the SiO_4 and Si_2O_7

groups) including the strongest peak at 914 cm^{-1} (Figure 7a) (Table 2 in Ref. 27). Since according to Wang *et al.*[113] the symmetric stretching vibration of $Si–O_b–Si$ type should be expected in the 750–450 cm^{-1} region, this mode was prescribed to the strong band at 599 cm^{-1} (it is absent in the Raman spectrum of the garnets where no bridging oxygen atoms are present).[21,113] The next strong band at 565 cm^{-1} was attributed to the $Si–O_b–Si$ bendings because it is present in the corresponding garnet spectra at close wavenumber and strong intensity (almandine, 565; spessartine, 548 cm^{-1}).

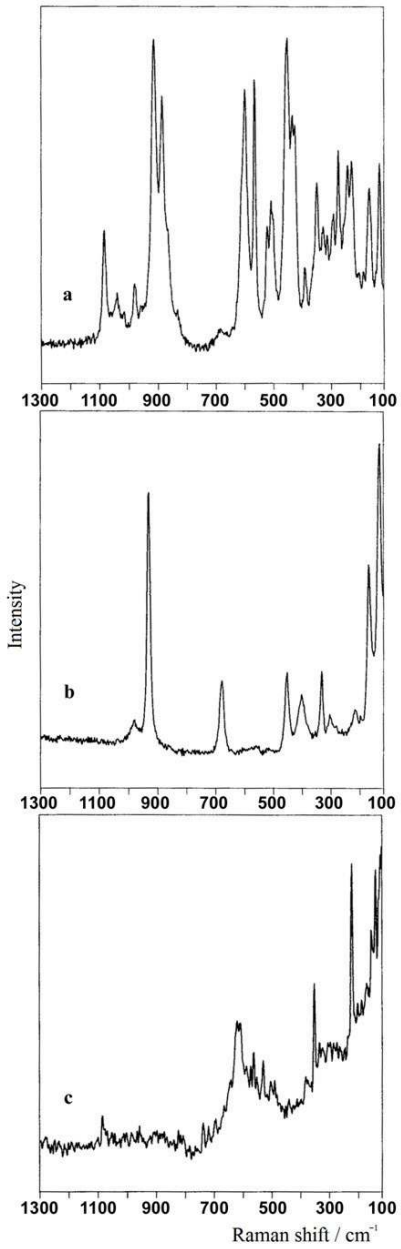

Figure 7. The dispersive Raman spectra of epidote (a), hemimorphite (b) and ilvaite (c) in the Si_2O_7 region (1300–100 cm^{-1}) excited with 514 nm.

The hemimorphite Raman spectrum is in a good agreement with the corresponding mineral spectrum published on Internet.[114] The number of bands in the 1100–800 cm^{-1} region (Figure 7b) (Table 3 in Ref. 27) is considerably smaller compared to the same region in epidote (Table 2 in Ref. 27). Namely, only two peaks due to the symmetric stretching $Si–O_{nb}$ vibrations are present in hemimorphite (7 in epidote), because only the vibrations of the Si_2O_7 groups could be attributed to the mentioned bands (there are no additional SiO_4 units as it is case in epidote). The very weak bands at 559 and 516 cm^{-1} as well as the medium band at 452 cm^{-1} probably arise from the $Si–O_b–Si$ bending modes (Table 3 in Ref. 27), and again, their number is less than in corresponding epidote spectrum (Table 2 in Ref. 27). According to the corresponding IR spectrum of hemimorphite, the band at 402 cm^{-1} is presumably due to the ν(Zn–O) mode.

Compared to the previously discussed Raman spectra of epidote and hemimorphite, the Raman spec-

Table 6. The most intense maxima and the crystallographic parameters derived from the X-ray powder diagram of the studied epidote mineral

h	k	l	d_{obs}	d_{cal}	d_{diff}
1	0	–1	3.9876	4.0068	–0.0192
1	0	–2	2.5258	2.5385	–0.0127
2	0	–2	2.0371	2.0323	0.0048
1	0	–3	1.7395	1.7356	0.0039
2	0	1	1.6489	1.6514	–0.0025
1	1	–3	1.4994	1.5023	–0.0029
0	2	0	1.4614	1.4609	0.0005
1	2	0	1.3861	1.3859	0.0002
3	1	–2	1.3587	1.3580	0.0007
2	0	2	1.3267	1.3276	–0.0009
0	2	–2	1.2658	1.2650	0.0008
1	2	–3	1.1566	1.1564	0.0002
2	2	1	1.1350	1.1347	0.0003
4	0	0	1.0866	1.0872	–0.0006
1	1	4	1.0287	1.0286	0.0001
3	1	2	1.0224	1.0221	0.0003
1	0	–6	0.9273	0.9273	0.0000
3	3	–1	0.9043	0.9044	–0.0001
1	1	5	0.9030	0.9031	–0.0001
6	0	–5	0.8410	0.8410	0.0000
4	2	2	0.8362	0.8360	0.0002

Unit Cell Par. (obs)	Unit. Cell. Par.[77]
a = 8.8891 Å	a = 8.980 Å
b = 5.6152 Å	b = 5.640 Å
c = 10.1466 Å	c = 10.220 Å
β = 115.48º	β = 115.4º
V = 457.206 Å^3	V = 467.58 Å^3; Z = 2
	Monoclinic ($P2_1/m$)

trum of ilvaite is of lower quality showing high noise-to-signal ratio and strong fluorescence (Figure 7c). According to the literature,[114] the Raman spectrum of this mineral has not been successfully collected because of its blackish color. The assignment of the bands is tentative and derived from the previously brought conclusions concerning the IR spectrum (Table 4 in Ref. 27).

X-ray Powder Diffraction Analysis

The X-ray powder analysis of the sorosilicate minerals, including the unit cell parameters determination, was performed for their identification purposes as well for checking the purity of the minerals. The obtained results show highly expressed similarities with the corresponding literature data,[101] confirming the authencity of the minerals (see Tables 6, 7 and 8).

Table 7. The most intense maxima and the crystallographic parameters derived from the X-ray powder diagram of the studied hemimorphite mineral

h	*k*	*l*	d_{obs}	d_{cal}	d_{diff}
1	1	0	3.3208	3.3223	–0.0015
0	2	0	2.7076	2.7088	–0.0012
0	1	1	2.3422	2.3426	–0.0004
2	0	0	2.1295	2.1295	0.0000
1	3	0	1.6907	1.6908	–0.0001
2	1	1	1.6011	1.6012	–0.0001
0	3	1	1.5185	1.5188	–0.0003
0	4	0	1.3992	1.3994	–0.0002
0	0	2	1.3420	1.3420	0.0000
3	0	1	1.2905	1.2907	–0.0002
2	3	1	1.2675	1.2675	0.0000
3	2	1	1.1876	1.1876	0.0000
3	3	0	1.1741	1.1743	–0.0002
2	0	2	1.1667	1.1670	–0.0003
4	0	0	1.1258	1.1257	0.0001
1	3	2	1.0929	1.0925	0.0004
0	4	2	1.0180	1.0181	–0.0001
3	4	1	0.9997	0.9997	0.0000
0	6	0	0.9905	0.9904	0.0001
5	3	0	0.8805	0.8804	0.0001

Unit Cell Par. (obs)	Unit. Cell. Par.[77]
a = 8.3661 Å	a = 8.370 Å
b = 10.7145 Å	b = 10.719 Å
c = 5.1150 Å	c = 5.120 Å
V = 458.50 Å^3	V = 459.36 Å^3; Z = 2
	Orthorhombic (*Imm*2)

Inosilicates (Chain Silicates)

Pyroxenes and Pyroxenoids – The pyroxene group is found to be the most important group in planetary mineral suites revealing the information about petrogenetic processes.[122] Recent studies exposed their dominant part as a major rock forming silicates on the surface of Mars.[123,124] In this context, determining the compositional and structural charactersitics of pyroxenes in rocks can be crucial to understand rocks petrogenesis.

Table 8. The most intense maxima and the crystallographic parameters derived from the X-ray powder diagram of the studied ilvaite mineral

h	*k*	*l*	d_{obs}	d_{cal}	d_{diff}
1	1	0	3.6777	3.6740	0.0037
0	2	0	3.2756	3.2772	–0.0016
1	1	1	2.3186	2.3167	0.0019
2	2	0	2.1292	2.1269	0.0023
1	3	0	1.9852	1.9864	–0.0012
2	1	1	1.7474	1.7462	0.0012
0	4	0	1.6748	1.6747	0.0001
2	3	0	1.5971	1.5976	–0.0005
0	0	2	1.5168	1.5162	0.0006
3	1	0	1.4893	1.4901	–0.0008
0	4	1	1.4783	1.4772	0.0011
1	1	2	1.4160	1.4161	–0.0001
1	2	2	1.3384	1.3395	–0.0011
2	0	2	1.2851	1.2852	–0.0001
2	4	1	1.2626	1.2628	–0.0002
1	3	2	1.2387	1.2386	0.0001

Unit Cell Par. (obs)	Unit Cell Par.[77]
a = 8.8226 Å	a = 8.780 Å
b = 13.0066 Å	b = 12.990 Å
c = 5.8460 Å	c = 5.850 Å
V = 670.844 Å^3	V = 667.21 Å^3; Z = 4
	Orthorhombic (*Pbnm*)

The pyroxenes are built up of single SiO_4 tetrahedral chains that extend parallel to the *c*-axis in a way that every next other tetrahedron alternates from the left side to the right side of the chain.[77] The repeat distance along the chains are two tetrahedra representing the *c*-unit cell parameter.[77] The structure of the studied pyroxenoids is very similar to the pyroxenes despite the fact that the chains of silicon tetrahedra are distorted or twisted. Namely, the repeat distance in the structure of bustamite is three, whereas in rhodonite five tetrahedra repeat the unit.[77]

Structural Data and XRPD Analysis

The chemical formula of the pyroxene could be derived from the general formula XYZ_2O_6, except for carpholite, $MnAl_2Si_2O_6(OH)_4$ (Table 9). The Z cations, (Si^{4+}, and rarely Al^{3+}), have tetrahedral coordination, whereas X cations (Ca^{2+}, Mn^{2+}, Na^{+}) occupy the M2 sites between the bases of the tetrahedra in somewhat distorted 6- or 8-fold coordination.[77] If M2 site has 6-fold coordination, the mineral has orthorhombic symmetry (carpholite), but if 8-fold coordination is produced, the

Table 9. The most important crystallographic features of the studied pyroxenes and pyroxenoids

Mineral	Crystal System	Unit cell parameters		Unit cell volume
		$\frac{a,b,c}{\text{Å}}$	$\frac{\alpha,\beta,\gamma}{\text{degree}}$	$\frac{\text{Unit cell volume}}{\text{Å}^3}$
Hedenbergite[125]	Monoclinic ($C2/c$)	$a = 9.827$ $b = 8.994$ $c = 5.261$	$\beta = 105.52$	448.0
Hedenbergite (This work)		$a = 9.8655$ $b = 9.0471$ $c = 5.2612$	$\beta = 104.98$	453.6
Johannsenite[126]	Monoclinic ($C2/c$)	$a = 9.978$ $b = 9.156$ $c = 5.293$	$\beta = 105.48$	466.0
Johannsenite (This work)		$a = 9.9771$ $b = 9.1576$ $c = 5.2905$	$\beta = 105.45$	465.9
Carpholite[127]	Orthorombic ($Ccca$)	$a = 13.86$ $b = 20.13$ $c = 5.12$		1428.5
Carpholite (This work)		$a = 20.2421$ $b = 13.8115$ $c = 5.1177$		1430.8
Rhodonite[128]	Triclinic ($P\bar{1}$)	$a = 9.758$ $b = 10.499$ $c = 12.205$	$\alpha = 108.58$ $\beta = 102.92$ $\gamma = 82.52$	1152.9
Rhodonite (This work)		$a = 10.5286$ $b = 12.1950$ $c = 9.8822$	$\alpha = 104.00$ $\beta = 97.96$ $\gamma = 71.28$	1163.5
Bustamite[129]	Triclinic ($P\bar{1}$)	$a = 15.41$ $b = 7.15$ $c = 13.82$	$\alpha = 89.98$ $\beta = 94.85$ $\gamma = 102.93$	1478.7
Bustamite (This work)		$a = 7.6857$ $b = 13.7719$ $c = 7.1231$	$\alpha = 90.51$ $\beta = 103.80$ $\gamma = 94.84$	729.3

symmetry is monoclinic (hedenbergite, ferrojohannsenite). The Y cations (Mg^{2+}, Mn^{2+}, Fe^{2+}, Al^{3+}) occupy 6-fold M1 structural sites between the apical oxygens of adjacent chains. The pairs of the tetra-hedral chains (*T*) whose apical oxygens face each other and the strip of octahedral (*O*) coordinated M1 cations produce so called *TOT I*-beams.[77]

Therefore, for identification purposes and checking of the mineral purity, the X-ray powder diagrams were recorded (see Tables 3 and 4 in Ref. 25). Generally, the results are in a good agreement with the corresponding literature data[101,125–129] (Table 9). Some additional peaks due to the quartz (Q) and siderite (S) as well as quartz (Q) and calcite (C) impurities are registered in ferrojohannsenite and rhodonite X-ray pattern, respectively.

Since the chemical composition of the studied minerals could vary substantially, it was determined by X-ray microprobe analysis (Table 1) whereas the k_0-INAA[130,131] was employed primarily to determine the trace elements (Table 2 in Ref. 25). Using X-ray microprobe analysis as well as XRD it is found that the min-

eral contemplated as augite is, in fact, hedenbergite since both minerals are isomorphous and belong in the Ca clinopyroxene group.

Infrared Spectral Study

Hedenbergite, $(Ca,Mg)(Fe,Mn)Si_2O_6$, and Ferrojohannsenite, $Ca(Fe,Mn)Si_2O_6$, from Sasa and Carpholite, $(Mn,Mg)Al_2Si_2O_6(OH)_4$, from Vrpsko. Several studies have been undertaken to interpret the IR spectra of Ca clinopyroxenes[81,132–134] and bustamite,[81,133] whereas the IR spectra of carpholite and rhodonite[81] have been presented but not discussed.

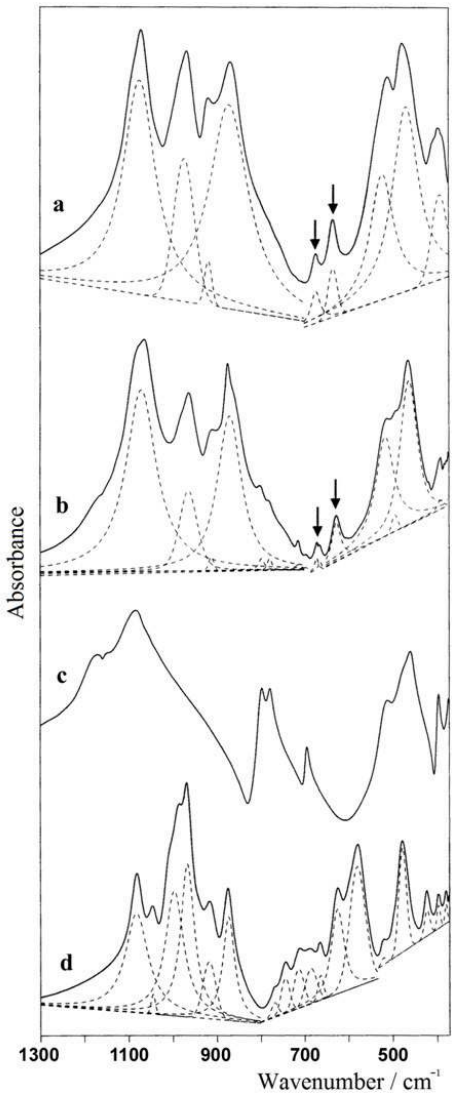

Figure 8. The IR spectra of the pyroxenes: hedenbergite (a), ferrojohannsenite (b) and carpholite (d) in the SiO_4 region (1300–370 cm^{-1}). The infrared spectrum of mineral quartz (c) is also given for comparison. The result of the curve fitting is given below each pyroxene spectrum. The bands from the deformations of the Si–O linkages in hedenbergite and ferrojohannsenite are marked by arrows.

The infrared spectra of hedenbergite and ferrojohannsenite, in the 1300–370 cm^{-1} region are presented in Figure 8a,b. As expected, the spectra show minor differences expressed by several very weak bands in 800–700 cm^{-1} region present in ferrojohannsenite. Furthermore, the spectra are rather similar with those reported in the corresponding literature data[81,132–134] being characterized with three well-separated band regions (Table 5 in Ref. 25).

The highest frequency region (1100–850 cm^{-1}) involves three strong and one weak band placed on the higher wavenumber side of the bands around 870 cm^{-1} (Figure 8a,b). Compared to the corresponding region in the nesosilicate minerals,[21] this spectral view is much complex. It is due to the fact that the pyroxene structure is built of the complex chains of SiO_4 anions whereas the SiO_4 building blocks in the nesosilicates are isolated. Such structural difference perturbs the degeneracy of the ν_2, ν_3 and ν_4 modes in the pyroxene infrared spectra[135] causing the appearance of larger number of IR bands as a result of the different bondings between the terminal (O_t) and bridging (O_b) oxygens to the Si atoms. In this context, the highest wavenumber peaks were assigned as the Si–O_t rather than Si–O_b modes. It is due to their greater force constants compared to the Si–O_b modes, because the Si–O_b motions are additionally shared between the adjacent tetrahedra. On the other hand, the wavenumbers of the bands in this region are nearly constant suggesting that chain vibrations are not particularly sensitive to the population of the cation sites.[133] It means that the observed bands in the 1100–850 cm^{-1} region are, to great extent, due to pure ν(O–Si–O) and ν(Si–O–Si) vibrations (Table 5 in Ref. 25).

Except the bands due to the deformations of the Si–O–Si linkages in the Ca clinopyroxenes that appear between 850 and 550 cm^{-1} (Figure 8a,b) (Table 5 in Ref. 25), the spectrum of the studied ferrojohannsenite exhibited several very weak bands at 798, 779, 714 and 696 cm^{-1}, not reported in the literature.[133] They were attributed to small content of quartz impurity in both samples supported by the fact that the wavenumbers strongly coincide with the corresponding ones (797, 779 and 694 cm^{-1}) in the quartz IR spectrum (Figure 8c and 10b). Furthermore, very weak band at 714 cm^{-1} observed in the spectrum of ferrojohannsenite was attributed to the carbonate impurity since ν_4 mode in siderite was observed nearly at the same wavenumber (see forthcoming discussion of the ferrojohannsenite Raman spectrum). It agrees with the results obtained by XRPD method.

The infrared spectrum of carpholite (Figure 8d) has not been studied by other authors, except being presented in the Nicodom atlas of minerals.[101] It was the only studied pyroxene that nominally contains two

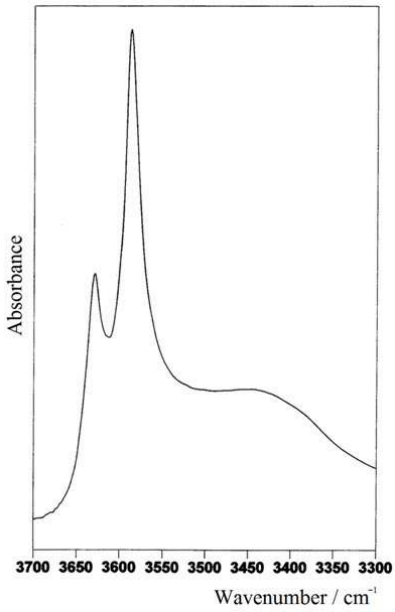

Figure 9. The IR spectrum of carpholite in the OH stretching region (3700–3300 cm^{-1}).

(crystallographically different) OH groups.[136] In accordance with it, two IR bands registered at 3630 and 3587 cm^{-1} (Figure 9) were attributed to the OH stretching vibrations (Table 6 in Ref. 25). The observed peaks in this region are in accordance with the literature data,[81] where no assignments are proposed.

The assignment of the bands in the 700–500 cm^{-1} region was much more complicated because, in addition to the Si–O–Si deformation modes, this region is also typical for the OH librational modes.[137] It causes the bands in this region to be overlapped and even partly coupled because the OH modes were expected to appear in wide region as a result of the present four OH groups in the structure. Taking these considerations into account, the weak bands at 711, 683, 661 and 623 cm^{-1} were assigned as predominantly bending Si–O–Si vibrations whereas the strong band at 577 cm^{-1} (absent in the studied non-hydroxide pyroxenes) probably is a result of out-of-plane bending OH vibrations.

Rhodonite, $(Mn,Ca)MnSi_2O_6$, from Petrova Reka and Bustamite, $(Mn,Ca,Fe)_3Si_3O_9$, from Sasa. The IR spectrum of rhodonite is only presented in the IR atlas of minerals[81] but not discussed. Its spectrum (Figure 10a) shows higher complexity compared to the corresponding spectra of both studied Ca clinopyroxenes (Figure 8a,b), the complexity being most pronounced in the 750–550 cm^{-1} region. Namely, despite the above mentioned bands originating from the quartz impurities (799, 780 and 697 cm^{-1}), five additional bands were observed and associated with deformations of the Si–O linkages (Table 7 in Ref. 25). In fact, the number of the

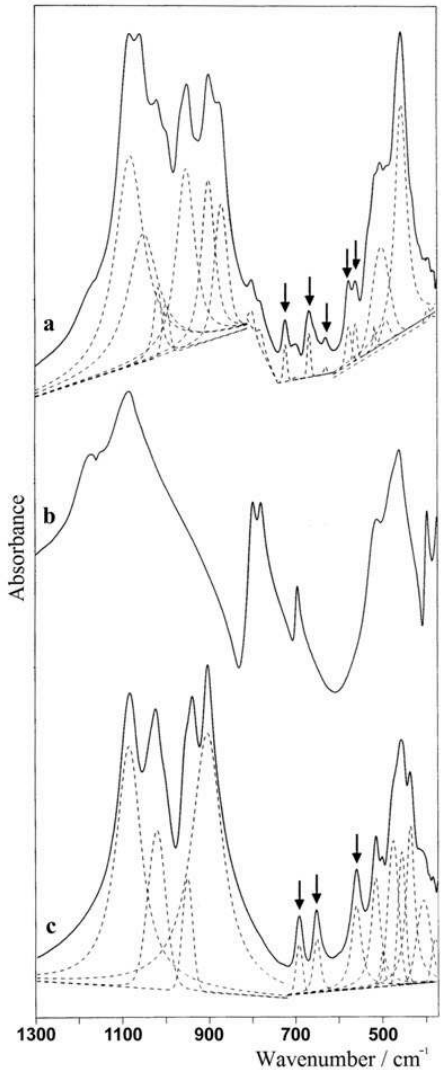

Figure 10. The IR spectrum of the pyroxenoids: rhodonite (a), bustamite (c) in the SiO_4 region (1300–370 cm^{-1}). The infrared spectrum of mineral quartz (b) is also given for comparison. The result of the curve fitting is given below each pyroxenoid spectrum. The bands from the deformations of the Si–O linkages in rhodonite and bustamite are marked by arrows.

bands in this region of any studied pyroxenoid provides an indication about the number of the tetrahedra in its repeating unit. It is in accordance with the structural data since the chains of silicon tetrahedra in rhodonite have repeat distance of five tetrahedra (see chapter structural data).

The IR spectrum of bustamite represents simplified pattern in term of smaller number of bands in stretching as well as in bending region of Si–O vibrations compared to rhodonite (Figure 10c). In its highest wavenumber region (characteristic for stretchings of Si–O modes), two pairs of strong bands were observed closely related to the literature[81,133] (Table 7 in Ref. 25).

Furthermore, only three bands in 700–550 cm^{-1} region associated with bending vibrations of the Si–O–Si linkages presumably reflects three tetrahedron repeat unit in bustamite structure.

The observed higher wavenumbers for the $\nu(XO_6)$ modes in the IR spectra of pyroxenes hedenbergite (469 cm^{-1}), ferrojohannsenite (463 cm^{-1}) and carpholite (475 cm^{-1}), compared to the lower wavenumbers of the corresponding mode in the spectra of pyroxenoids rhodonite (455 cm^{-1}) and bustamite (458 cm^{-1}) (Tables 5–7 in Ref. 25) could, at some extent, differentiate between the pyroxenes, on the one hand, and pyroxenoids, on the other.

Raman Spectral Study

Various authors have studied the Raman spectra of Ca clinopyroxenes[138] and rhodonite.[113,124,139,140] The Raman data for ferrojohannsenite, bustamite and carpholite, to the best of our knowledge, have not been reported in the literature.

Hedenbergite, $(Ca,Mg)(Fe,Mn)Si_2O_6$, and Ferrojohannsenite, $Ca(Fe,Mn)Si_2O_6$, from Sasa. The Raman spectra of hedenbergite and ferrojohannsenite are presented in Figure 11a,b and the band assignments listed in Table 8 of Ref. 25. The most characteristic feature was a very strong band around 1010 cm^{-1} associated with the shoulder around 1030 cm^{-1}. They were related to the ν_{as}(Si–O–Si) and ν_{as}(O–Si–O) modes[124,138,141] involving the non-bridging instead of the bridging oxygen atoms due to expected stronger force constants of the former ones (latter ones are additionally shared between the adjacent tetrahedra).

Three additional bands at 1084, 713 and 277 cm^{-1}, not typical for clinopyroxenes, were observed in the ferrojohannsenite Raman spectrum (Figure 11b) (Table 8 in Ref. 25). They arise from the present carbonate impurity (also detected in the powder X-ray diagram and IR spectrum of the same mineral). Similarly, the medium band at 461 cm^{-1} in the spectrum of ferrojohannsenite predominantly originate from the quartz impurity, although, to some extent, it is mixed and overlapped with the Si–O–Si deformation observed in the spectrum of Mg-rich clinopyroxene (463 cm^{-1}).[138,141]

The very strong band around 655 cm^{-1} in the Raman spectra of hedenbergite and ferrojohansenite (Figure 11a,b) is related to the fact that *C*2/*m* clinopyroxenes posses only one symmetrically distinct tetrahedral site (orthopyroxenes posses two distinct sites).[142] On the other hand, although different cations could be substituted in the unique tetrahedral site in hedenbergite, the wavenumber of the strongest band does not significantly differ compared to ferrojohannsenite. It is in accordance with the results of Mernagh and Hoatson[141] who found that the polyhedral clusters do not substantially change in size and shape as a response to substitution of different cations.

In the line with the previous assignments carried out for the corresponding modes in the case of amphiboles,[26] the moderately intense bands around 370 and 300 cm^{-1} in hedenbergite and ferrojohannsenite spec-

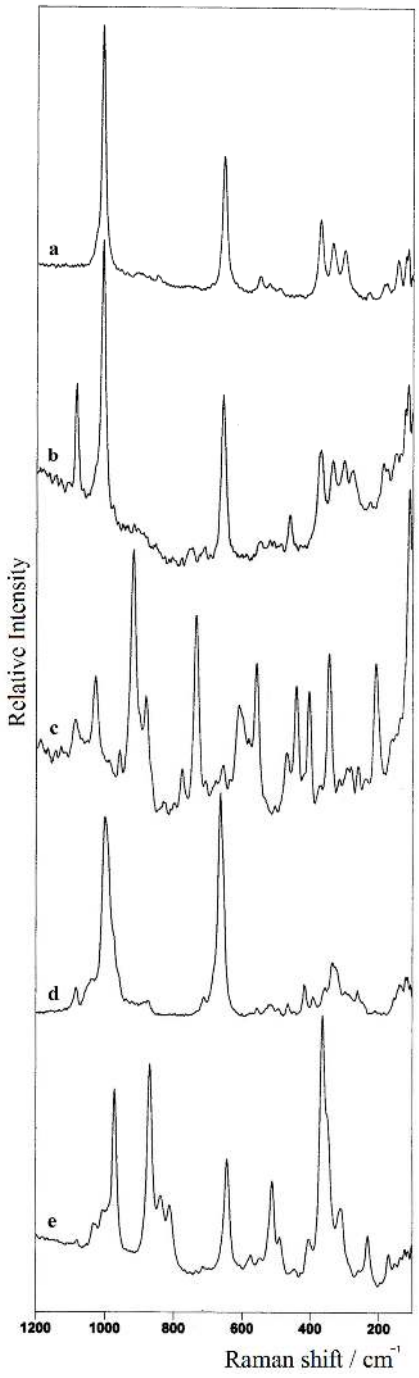

Figure 11. The dispersive Raman spectra of the pyroxenes: hedenbergite (a), ferrojohannsenite (b), carpholite (c) and pyroxenoids: rhodonite (d), bustamite (e) in the SiO_4 region (1200-100 cm^{-1}) excited with 514 nm.

trum appeared from the Fe–O and Mn–O displacements, whereas the remaining two bands around 330 and 230 cm^{-1} are due to the translations involving Ca–O (and additionally Mg–O in hedenbergite) displacements (Figure 11a,b) (Table 8 in Ref. 25). As it was already stated, the 277 cm^{-1} band in the spectrum of ferrojohannsenite arises from the carbonate impurities.

Rhodonite, $(Mn,Ca)MnSi_2O_6$, from Petrova Reka and Bustamite, $(Mn,Ca,Fe)_3Si_3O_9$, from Sasa. The Raman spectrum of carpholite (Figure 11c) differs significantly from the other studied Raman spectra, but exhibits strong similarity with the correspondding IR spectrum (Table 6 in Ref. 25). The similarity was expressed in the appearance of IR counterparts of Raman bands (IR-Raman doublets), even though the studied mineral has centre of inversion (*Ccca* space group, Table 9). However, our previous study on the vibrational spectra of some clinoamphibole minerals that posses centre of inversion in the structure also showed IR-Raman doublets.[26] It was revealed that if the main vibrational units are arranged to form layers, the symmetry of the layer dominates over the symmetry of the crystal. In fact, the stacking sequence of the layers determines the symmetry and the activity of the normal modes (the symmetry of the present *TOT I*-strips in its structure dominates over the crystal symmetry). Therefore, the assignment of the Raman bands was generally derived from the IR conclusions.

The Raman spectra of the studied pyroxenoids rhodonite and bustamite are presented in Figure 11d,e, whereas the comparison with the corresponding literature data for rhodonite including the band assignments for both minerals is given in Table 9 of Ref. 25.

According to Mills *et al.*[140] the Raman spectrum of rhodonite could be interpreted assuming that its structure is similar to the structure of the nesosilicates where SiO_4 tetrahedra are not bonded to other tetrahedra (and the large cation perturbs the tetrahedral SiO_4 units). Applying the approximation for the structure of the studied pyroxenoids, ν_1 symmetric stretching mode and ν_2 doubly degenerate (out-of-plane) bending mode would be Raman active, whereas ν_3 triply degenerate antisymmetric stretching mode and ν_4 triply degenerate (in-plane) bending mode would be expected in the IR spectrum.

The 1100–850 cm^{-1} region of the rhodonite Raman spectrum (Figure 11d) shows strong similarity with the literature data.[113,140] Some extent of spectral similarity with the corres-ponding bustamite spectrum was also observed (Figure 11d,e). Consequently, the strong bands at 1000 cm^{-1} in rhodonite and at 972 cm^{-1} in bustamite were assigned as the ν_1 symmetric stretching mode. The wavenumbers of the assignment of the bands (Table 9 in Ref. 25) were in accordance with the corresponding one registered in our Raman study of the nesosilicate minerals.[21] It supports the approximation of Mills *et al.*[140] that the structure of the pyroxenoids could be considered as similar to the structure of nesosilicates in order to simplify and make the assignment of the Raman bands possible.

The 900–800 cm^{-1} spectral region represents very discriminative pattern. Namely, two bands at 839 and 812 cm^{-1} were observed for bustamite, whereas they were absent in the rhodonite spectrum. Furthermore, the strong absorption at 869 cm^{-1} was observed in bustamite Raman spectrum as a result of Si–O stretchings, whereas only a weak band was observed in the spectrum of rhodonite at 875 cm^{-1} as a counterpart. These differences could not be explained at this stage of the work, although the authenticity of the minerals was confirmed by the X-ray powder diffraction.

Taking into consideration the approximation of the pyroxenoid structure with the nesosilicate one, the strongest band at 664 cm^{-1} (rhodonite) and 644 cm^{-1} (bustamite) were attributed to the ν_4 bending mode (Table 9 in Ref. 25). On the bases of the IR assignments, the bands around 490, 465 and 445 cm^{-1} were prescribed to the ν(Mn–O) modes, whereas the maxima around 420, 280 and 260 cm^{-1} are the components from the ν_2 bending modes.[140] It was apparent that the large number of bands in this region could be taken as an evidence for the non-equivalence of the SiO_4 tetrahedra in both pyroxenoid structures. The remaining maxima (400, 360 and 340 cm^{-1}) could be prescribed to the stretching vibrations of the XO_6 tetrahedra (X = Ca in bustamite, Mn and Ca in rhodonite).

Amphiboles – Similarly to the structure of the single chain inosilicate minerals (pyroxenes) where two O^{2-} anions per tetrahedra are shared, in the structure of amphiboles the remaining tetra-hedra share three oxygen anions, forming thereby the double chains of SiO_4 tetrahedra as their main structural units.[77] These double chains extend parallel to the *c*-axis being stacked in an alternating way. Such type of geometry produces 5 different structural sites marked as M1, M2 and M3 octahedral sites positioned between the chains, and larger M4 and A sites between the bases. The location of both chains of tetrahedra (*T*) arranged facing each other leads to octahedral (*O*) coordination of the smaller M1, M2 and M3 cations. The result is the formation of so called *TOT* strips that are extended parallel to *c*-axis and are stacked atop each other in the *a* direction to produce M4 and A sites between the bases of the tetrahedra.

The amphibole minerals have the general formula $W_{0-1}X_2Y_5Z_8O_{22}(OH)_2$ (W = Na, K; X = Na, Ca; Y =

Mg, Fe^{2+}, Fe^{3+}, Al; Z = Si, Al). Their chemical composition is not necessarily fixed due to the possibility to form solid solution series with other minerals being their end-members (for example, tremolite–ferro-actinolite series, $Ca_2Mg_5Si_8O_{22}(OH)_2$ - $Ca_2Fe_5Si_8O_{22}(OH)_2$).

The vibrational (IR and Raman) spectroscopy as well as XRPD are used in order to identify and characterize the following amphibole minerals originating from the R. Macedonia: glaucophane, $Na_2(Mg,Fe)_3(Fe,Al)_2Si_8O_{22}(OH)_2$; actinolite, $Ca_2(Mg,Fe)_5Si_8O_{22}(OH)_2$; hornblende, $(Na,K)_{0-1}Ca_2(Mg,Fe^{2+},Fe^{3+},Al)_5(Si,Al)_8O_{22}(OH)_2$ and arfvedsonite, $Na_2(Na,K)(Mg,Fe,Ca)_4(Fe,Al)Si_8O_{22}(OH)_2$.

Several studies have been undertaken to observe the vibrational spectra of glaucophane,[143–145] tremolite-actinolite,[146–151] arfvedsonite[81,152,153] and hornblende.[81,145,154] The Raman data for arfvedsonite, to the best of our knowledge, have not been published yet.

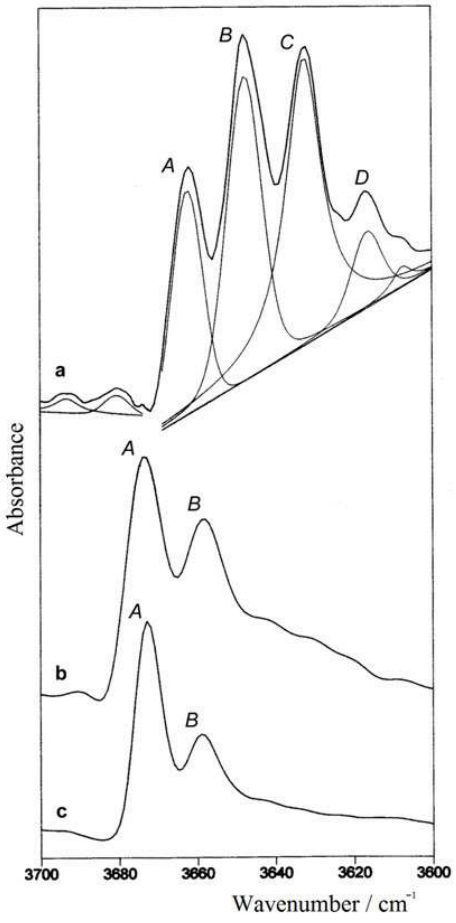

Figure 12. The powder IR spectrum of glaucophane from Vodno (a) and actinolite from Veselčani (b) and Košino (c) in the OH stretching region (3700–3600 cm^{-1}). The result of the curve fitting is given below the glaucophane spectrum.

Infrared and Raman Spectral Study

Glaucophane, $Na_2(Mg,Fe)_3(Fe,Al)_2Si_8O_{22}(OH)_2$, from Vodno. The strength of O–H bond slightly differs when different cations are coordinated to the OH group. Thus, the implementation of simple harmonic model of different M^{2+}–O oscillators would result in frequency shifting of the band in the spectrum. According to Ernst and Wai,[143] in glaucophane and any other amphibole type of mineral, each hydroxyl group (always located in the anion *O* site), is coordinated by three M^{2+} cations – two lying in M1 site and one in M3 site. If at least two of the cations are different, it would lead to at least two different M^{2+}–OH coordinations that, on the other hand, would reflect in different combinations of the OH stretching bands. On the other hand, the Fe^{3+} cations sometimes could replace M^{2+} cation, but at the same time the Al replaces Si in order to maintain the charge balance unchanged.

The RT glaucophane IR spectrum is presented in Figure 12a. Four well-resolved bands at 3662, 3648, 3632 and 3616 cm^{-1} (*A–D* notation) appear in the spectrum being in very good agreement with the observation by Ernst and Wai.[143] On the other hand, the band at 3616 cm^{-1} is not registered in the corresponding work by Gillet *et al.*[144] Since the replacement of Mg^{2+} with Fe^{2+} within the octahedral sites (two M1 and one M3) tends to shift the stretching O–H band towards the lower frequencies[145,135] the peak at 3616 cm^{-1} (denoted as *D* band) could be prescribed to the combination where M sites are occupied only by (three) Fe^{2+} cations. The additional very weak band at 3608 cm^{-1} (Figure 12a) (Table 2 in Ref. 26), probably arises from OH stretching related to the cation combination involving replacement of one Fe^{2+} with one Fe^{3+} cation in the M site. In the line with the assumption, the peak at 3662 cm^{-1} (*A* band) arises from the combination where three Fe^{2+} cations are substituted with Mg^{2+}, whereas the bands at 3648 and 3632 cm^{-1} are due to the cation combination of two Mg^{2+} and one Fe^{2+} as well as one Mg^{2+} and two Fe^{2+} cations on the three M sites (*B* and *C* band, respectively). It implies that the IR spectrum of glaucophane in the OH region serves as a powerful pattern to confirm the results from chemical analysis (Table 1) that studied glaucophane sample contains magnesium and iron cations in the octahedral M1 and M3 sites. Moreover, the spectrum is complicated by the appearance of additional very weak peaks at 3693 and 3680 cm^{-1} (Figure 12a) that are not mentioned in the literature (Table 2 in Ref. 26). Probably their origin could be related to the OH vibrations involving the presence of cation(s) on the A structural sites (Na and K, see Table 1), as it is the case in Mg-arfvedsonite (3680 to 3720 cm^{-1}).[151]

The RT and LNT spectra of glaucophane sample presented in 1300–370 cm^{-1} region (Figure 13a,b,

respectively) are in great accordance with the literature data.[144] The interpretation of the spectra in this region is generally based on the bands dominantly arising from the vibrations of the main structural features - Si_8O_{22} groups and from the cation-oxygen bondings. Having in mind the corresponding literature spectrum,[144] an attempt to summarize and assign the bands in this region is shown in Table 2 of Ref. 26.

Similarly to the assignment of the IR spectrum, the bands in the 1100–950 cm^{-1} and 910–670 cm^{-1} regions in the Raman spectrum of glaucophane presented in Figure 14a, are ascribed to the antisymmetric and symmetric Si–O–Si and O–Si–O vibrations from the SiO_4 chain building units, respectively (Table 2 in Ref. 26).

Although the centre of inversion is present in the structure of glaucophane (*C*2/*m* space group) and other studied amphiboles, as it was previously mentioned in the case of pyroxenes, the so called IR-Raman doublets appeared (the symmetry of the *TOT* strips dominates over the symmetry of the crystal).

Actinolite, $Ca_2(Mg,Fe)_5Si_8O_{22}(OH)_2$, from Košino. According to Nesse,[77] solutions with more than 90 % Mg are called tremolite, between 90 % and 50 % actinolite and less than 50 % Mg, ferro-actinolite. Having in mind the varying chemical composition in the series of these minerals, it is important to find out whether IR spectroscopy could discriminate between the members of this series *i.e.* whether some spectral differences between tremolite and (ferro-)actinolite could be observed.

The RT spectra of the actinolite samples in the OH stretching region (3700–3600 cm^{-1}) are presented in Figure 12b,c, whereas their spectra in the lower-

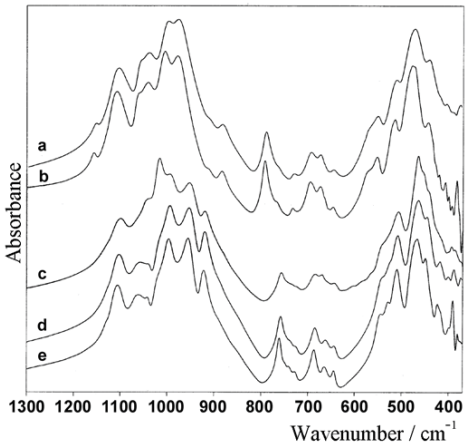

Figure 13. The powder IR spectrum of glaucophane from Vodno (a - RT; b - LNT), actinolite from Veselčani (c - RT) and Košino (d - RT; e - LNT) in the SiO_4 region (1300–370 cm^{-1}).

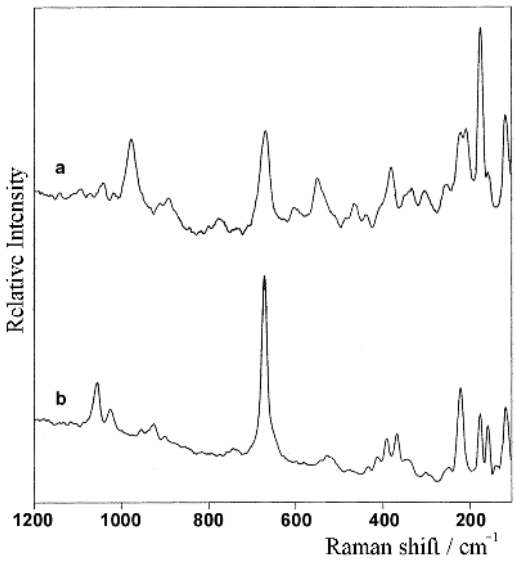

Figure 14. The dispersive Raman spectrum of glaucophane from Vodno (a) and actinolite from Košino (b) in the SiO_4 region (1200–100 cm^{-1}) excited with 532 nm.

frequency region from 1300 to 370 cm^{-1} are given in Figure 13c,d, including the LNT spectrum of the sample from Košino (Figure 13e).

According to Ishida *et al.*,[147] the ν(OH) bands in tremolite-ferro-actinolite series [$Ca_2Mg_5Si_8O_{22}(OH)_2$ - $Ca_2Fe_5Si_8O_{22}(OH)_2$] are expected to appear in three regions of descending order of frequency: (i) only one composite band appears in the samples with partly filled A sites, (ii) four main OH-stretching bands appear when A sites are vacant, and (iii) weak bands below 3460 cm^{-1} appear and their intensity relations does not coincide with those of the principle bands. Moreover, similarly to the previous discussion concerning the bands in the stretching OH region of glaucophane spectrum, very weak band at 3690 cm^{-1} is observed only in the spectrum from Veselčani sample, probably due to the slightly filled A sites. However, the main characteristic of the OH stretching region is the appearance of two well-developed weak bands at 3673 (*A*) and 3659 cm^{-1} (*B*) (Figure 12b,c) (Table 3 in Ref. 26). Depending on the presence and/or absence of Fe^{2+} in M1 and M3 sites, the number of bands could range from one in tremolite up to four in ferro-actinolite samples.

It should be noted that the highest-frequency OH stretching band (*A*) is ascribed to the vibration representing the state when three Mg^{2+} cations are present, one in M3 site and two in M1 sites. When corresponding sites are occupied with three Fe^{2+} cations the band is expected at lowest OH frequency, 3625 cm^{-1} (*D* band).[147,148,135] Since this band is absent in our IR spectra, it could imply that the studied samples are not (ferro-)actinolite. Moreover, the remaining band at 3659

cm^{-1} is ascribed to the OH vibration where either M3 or one of the M1 sites is occupied with Fe^{2+}. Also, no band is observed around 3643 cm^{-1} that corresponds to (Mg,Fe^{2+},Fe^{2+})–OH configuration (*C*),[148,155] supporting the statement that the studied samples are actinolites. It is in accordance with the results obtained from the chemical analysis (Table 1).

Contrary to the OH stretchings, both RT IR spectra of samples from Veselčani and Košino in the 1300–370 cm^{-1} region (Figure 13c,d) show less differences in the number as well as in the separation and intensity of the bands for various cation substitutions[149,150] (Table 3 in Ref. 26). Thereby, this region could not distinguish between actinolite and tremolite mineral species because the discriminating (analytical) bands either have weak intensity or appear as shoulders.

The Raman spectrum of the studied mineral from Košino in the 1200–100 cm^{-1} region is shown on Figure 14b. The highest-frequency peaks observed at 1056, 1026 and 954 cm^{-1}, also present in the literature for both actinolite and tremolite minerals,[146,149] are attributed to the antisymmetric Si–O modes (Table 4 in Ref. 26). The

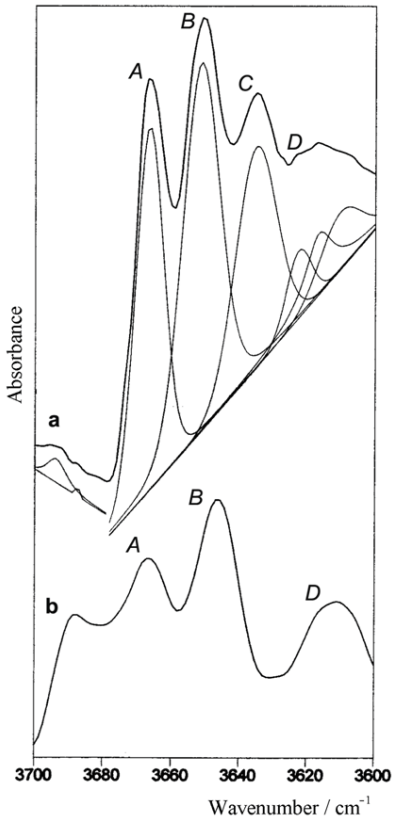

Figure 15. The powder IR spectrum of arfvedsonite from Alinci (a) and hornblende from Pelagon (b) in the OH stretching region (3700–3600 cm^{-1}). The result of the curve fitting is given below the arfvedsonite spectrum.

symmetric Si–O stretchings are represented by the weak peaks at[926, 899] (not found in the literature) and 744 cm^{-1} as well as the strongest peak in the spectrum at 672 cm^{-1} due to the symmetric Si–O–Si stretching.

The bands due to the Si–O–Si bendings (527, 517, 477 and 433 cm^{-1}) could not discriminate between actinolite and tremolite since they are observed at almost identical wavenumbers (except the 477 cm^{-1} band that is not registered).[149] Non-discriminative are also weak bands assigned as M–O stretching vibrations observed at 413, 391, 368 and 346 cm^{-1} (Table 4 in Ref. 26).

As a bottom line, it could be concluded that, compared to the Raman technique, IR spectroscopy provides better results in the identification of the studied samples enabling to exhibite that it is actinolite rather than tremolite or (ferro-)actinolite.

Arfvedsonite, $Na_2(Na,K)(Mg,Fe)_4(Fe,Al)Si_8O_{22}(OH)_2$, *from Alinci.* Contrary to both previously studied minerals (glaucophane and actinolite), arfvedsonite contains Na cations that occupy A structural sites. Its chemical formula could also show variation represented by the Mg–Fe cation substitution, the complete substitution of Fe^{2+} with Mg^{2+} being known as magnesio-arfvedsonite mineral.[155]

In order to identify the studied mineral (arfvedsonite or magnesio-arfvedsonite), the OH stretchings in the IR spectrum are separately presented and discussed (Figure 15a) (Table 5 in Ref. 26). The spectral view in this region is rather complex being represented by two very weak bands above 3680 cm^{-1} as well as four weak bands (and two shoulders) ranging from 3680 to 3600 cm^{-1}. According to Ishida and Hawthorne,[152] both highest frequency peaks are ascribed to the stretchings of the OH groups adjacent to a filled A site, whereas the six lower frequency ones are ascribed to the stretching vibrations of the OH groups adjacent to a vacant A site being of (M1M1M3)–OH–A type (A = A-site alkali ions) and (M1M1M3)–OH–□ type (□ = vacancy), respectively. Namely, maxima at 3666, 3651, 3635 and 3623 cm^{-1} (*A–D* bands) represent the OH stretchings with the following cation combinations $Mg^{2+}Mg^{2+}Mg^{2+}$, $Mg^{2+}Mg^{2+}Fe^{2+}$, $Mg^{2+}Fe^{2+}Fe^{2+}$ and $Fe^{2+}Fe^{2+}Fe^{2+}$, respectively (Table 5 in Ref. 26). The substantial broadening of the *A–D* series of bands by substitution of Fe^{3+} by Al^{3+} in riebeckite[153] is also registered in our spectrum (Figure 15a). Namely, the smaller six-fold coordinated Fe^{3+} cations are also generally concentrated in M2 sites.[143] Therefore, the lowest frequency OH stretching peaks at 3617 and 3610 cm^{-1} are prescribed to the $Fe^{2+}Fe^{2+}Fe^{3+}$ and $Fe^{2+}Fe^{3+}Fe^{3+}$ cation combinations, respectively, being in accordance with the literature data for actinolite mineral[147] (3618 and 3611 cm^{-1}). The ν(OH) region has shown that studied mineral contains

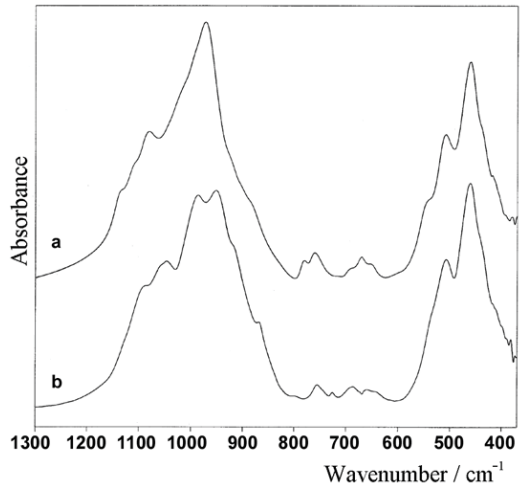

Figure 16. The powder IR spectrum of arfvedsonite from Alinci (a) and hornblende from Pelagon (b) in the SiO_4 region (1300–370 cm^{-1}).

both Mg^{2+} and Fe^{2+} cations and its chemical composition is closer to the magnesio-arfvedsonite than to arfvedsonite endmember (confirmed by chemical analysis, Table 1).

Although the IR spectrum below 1300 cm^{-1} (Figure 16a) is very similar to the corresponding spectrum of arfvedsonite published in the atlas from Nicodom,[81] to the best of our knowledge, no assignment has been found in the literature for this region. Its interpretation is based on the previous study of the corresponding spectra of glaucophane and actinolite being summarized in Table 5 of Ref. 26.

The Raman spectrum in the 1200–100 cm^{-1} region is shown on Figure 17a. Here it should be pointed out that, to the best of our knowledge, no Raman data have been found in the literature for this mineral specie. Since the previously discussed IR-Raman doublets are observed in the vibrational spectra of the series of the studied amphibole minerals, the interpretation of the Raman spectrum is based on the assignment of its IR bands. The Raman bands could be classified into five groups. The highest-frequency peaks, observed in 1060–890 cm^{-1} region, are attributed to the antisymmetric Si–O modes, whereas the bands ascribed to the symmetric Si–O stretchings give rise to the maxima (with variable intensity) between 820 and 610 cm^{-1} (Table 5 in Ref. 26). The most prominent band due to the Si–O–Si bendings (600–400 cm^{-1}) is the strong peak observed at 539 cm^{-1}, whereas the M–O translations are manifested by three maxima registered at 370, 335 and 317 cm^{-1}. The peaks due to the external modes appear in the lowest-frequency region below 260 cm^{-1}.

Hornblende, $(Na,K)_{0-1}Ca_2(Mg,Fe^{2+},Fe^{3+},Al)_5(Si,Al)_8O_{22}(OH)_2$, *from Pelagon.* The chemical complexity of this mineral[145] leads to the appearance of more than four bands in the OH stretching region with a corresponding loss of resolution. In the presented IR spectrum of the studied hornblende mineral (Figure 15b) four broad weak bands are registered (Table 6 in Ref. 26) being in accordance with the literature data.[154] Obviously, it is clearly seen from the spectrum that bands have larger full-width at half height (FWHH) (Figure 15b) compared to the corresponding bands in the previously discussed amphiboles (for example, arfvedsonite, see Figure 15a). It could be taken as an indication that the hornblende exhibits great variations in complexity, matching its wide compositional range. The assignment of the IR bands in the 1100–370 cm^{-1} region is in agreement with the assignment for the IR spectrum of previously discussed amphiboles (Table 6 in Ref. 26).

The Raman spectrum of hornblende (Figure 17b) is, with some clearly observable exceptions, similar to the corresponding literature data.[156] The major discrepancies concern to the medium and strong peaks at 611, 466 and 330 cm^{-1} that are absent in the corresponding literature spectrum[156] (Table 6 in Ref. 26). On the other hand, despite the great similarity between the IR spectra (Figure 16), suprisingly, the Raman spectra of the studied arfvedsonite and hornblende minerals (Figure 17) show expressed differences. They are mainly observed in the symmetric Si–O–Si stretching region (870–600 cm^{-1}) where instead of the weak band in the spectrum of arfvedsonite (at 610 cm^{-1}), strong band in our hornblende spectrum is registered. However, according to the assignment of the Raman spectrum of arfvedsonite mineral (sharing the same crystal structure with hornblende), this band is attributed to the fundamental

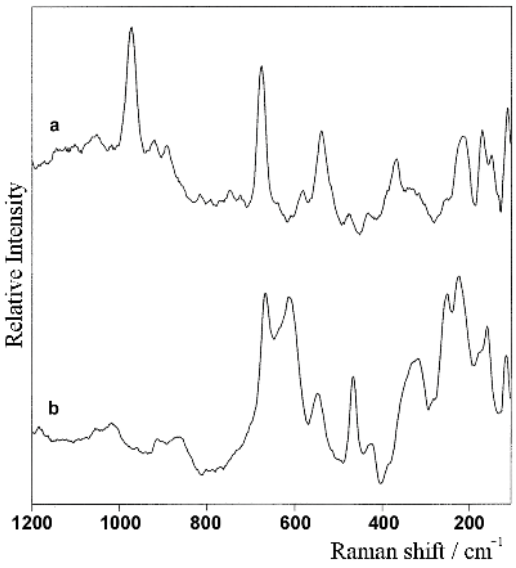

Figure 17. The dispersive Raman spectrum of arfvedsonite from Alinci (a) and hornblende from Pelagon (b) in the SiO_4 region (1200–100 cm^{-1}) excited with 532 nm.

Table 10. The most intense maxima and the crystallographic parameters derived from the X-ray powder diagram of studied glaucophane mineral

h	*k*	*l*	d_{obs}	d_{cal}	d_{diff}
0	2	0	4.4793	4.4751	0.0042
–1	1	0	4.1516	4.1472	0.0044
–1	1	1	2.4614	2.4607	0.0007
–1	3	1	1.9649	1.9642	0.0007
1	3	1	1.7399	1.7398	0.0001
–2	4	0	1.6581	1.6587	–0.0006
–3	1	0	1.5823	1.5809	0.0014
1	5	1	1.4081	1.4075	0.0006
–2	0	2	1.3262	1.3258	0.0004
–3	5	1	1.2169	1.2168	0.0001
–3	1	2	1.1958	1.1963	–0.0005
2	6	1	1.1516	1.1515	0.0001
2	0	2	1.1117	1.1116	0.0001
3	5	1	1.0846	1.0852	–0.0006

Unit Cell Par. (obs)	Unit Cell Par.[157]
a = 9.5803 Å	a = 9.541 Å
b = 17.8197 Å	b = 17.74 Å
c = 5.3106 Å	c = 5.295 Å
β = 103.64º	β = 103.67º
V = 881.055 Å^3	V = 870.83 Å^3; Z = 2
	Monoclinic ($C2/m$)

Table 11. The most intense maxima and the crystallographic parameters derived from the X-ray powder diagram of studied hornblende mineral

h	*k*	*l*	d_{obs}	d_{cal}	d_{diff}
0	2	0	4.5336	4.5284	0.0052
–1	1	0	4.2342	4.2335	0.0007
–1	1	1	2.4853	2.4859	–0.0006
2	0	0	2.4156	2.4158	–0.0002
0	4	0	2.2891	2.2896	–0.0005
0	2	1	2.2593	2.2599	–0.0006
1	1	1	2.0298	2.0301	–0.0003
–1	3	1	1.9860	1.9850	0.0010
0	4	1	1.7380	1.7379	0.0001
1	3	1	1.7356	1.7353	0.0003
–2	4	0	1.6865	1.6859	0.0006
–3	1	0	1.6145	1.6150	–0.0005
2	2	1	1.5220	1.5215	0.0005
–3	3	0	1.4613	1.4613	0.0000
–3	3	1	1.4312	1.4312	0.0000
1	5	1	1.4101	1.4108	–0.0007

Unit Cell Par. (obs)	Unit Cell Par.[158]
a = 9.8759 Å	a = 9.887 Å
b = 18.0337 Å	b = 18.174 Å
c = 5.3000 Å	c = 5.308 Å
β = 105.24º	β = 105.0º
V = 910.748 Å^3	V = 921.28 Å^3; Z = 2
	Monoclinic ($C2/m$)

Table 12. The most intense maxima and the crystallographic parameters derived from the X-ray powder diagram of studied actinolite mineral

h	*k*	*l*	d_{obs}	d_{cal}	d_{diff}
0	2	0	4.5527	4.5436	0.0091
–1	1	0	4.2300	4.2297	0.0003
–1	1	1	2.4733	2.4702	0.0031
0	4	0	2.2953	2.2971	–0.0018
–2	2	0	2.1430	2.1422	0.0008
–1	3	1	1.9812	1.9796	0.0016
0	4	1	1.7392	1.7393	–0.0001
–2	4	0	1.6865	1.6872	–0.0007
–3	1	0	1.6134	1.6121	0.0013
–3	1	0	1.6094	1.6121	–0.0027
–1	5	1	1.5258	1.5262	–0.0004
–3	3	0	1.4600	1.4601	–0.0001
–3	3	1	1.4253	1.4243	0.0010
1	5	1	1.4144	1.4138	0.0006
–2	0	2	1.3303	1.3295	0.0008
–3	5	0	1.2606	1.2607	–0.0001
–3	5	1	1.2387	1.2390	–0.0003
–4	2	0	1.2214	1.2210	0.0004

Unit Cell Par. (obs)	Unit Cell Par.[159]
a = 9.8301Å	a = 9.84 Å
b = 18.0945 Å	b = 18.1 Å
c = 5.2738 Å	c = 5.28 Å
β = 104.68º	β = 104.7º
V = 907.421 Å^3	V = 909.61 Å^3; Z = 2
	Monoclinic ($C2/m$)

Si–O–Si stretching vibration (from the SiO_4 tetrahedra within the chains). Similar intensity disproportion is also registered between the corresponding peaks at around 470 and 330 cm^{-1} observed in the Raman spectra of arfvedsonite and hornblende. On the other hand, the highest-frequency peaks above 900 cm^{-1} in the Raman spectrum of hornblende, ascribed to antisymmetric Si–O–Si and O–Si–O vibrations from the SiO_4 units, are in agreement with the literature data (Table 6 in Ref. 26).

In general, it could be concluded that in the case of amphiboles, the intensity and especially the number of the IR bands in the ν(OH) region serve for exact mineral identification. It is based on the presence of different Y cations in various octahedral sites (M1 and M3) which is manifested by different spectral view. However, variation of the extent of the sensitivity to impurities between both vibrational techniques justifies their simultaneous application confirming that they are complementary techniques.

X-ray Powder Diffraction Study

The identification of the studied amphibole minerals by vibrational spectroscopy was undoubtedly confirmed by PXRD technique. Namely, the most intense maxima in

Table 13. The most intense maxima and the crystallographic parameters derived from the X-ray powder diagram of studied arfvedsonite mineral

h	*k*	*l*	d_{obs}	d_{cal}	d_{diff}
0	2	0	4.5336	4.5257	0.0079
–1	1	0	4.2462	4.2572	–0.0110
0	0	1	2.6113	2.6115	–0.0002
–1	3	0	2.5779	2.5779	0.0000
2	0	0	2.4333	2.4333	0.0000
0	4	0	2.2880	2.2883	–0.0003
0	2	1	2.2747	2.2747	0.0000
–2	2	0	2.1560	2.1557	0.0003
1	1	1	2.0632	2.0627	0.0005
–2	0	1	2.0508	2.0508	0.0000
–1	3	1	1.9795	1.9794	0.0001
1	3	1	1.7548	1.7546	0.0002
0	4	1	1.7436	1.7438	–0.0002
–2	4	0	1.6911	1.6909	0.0002
–3	1	0	1.6260	1.6259	0.0001
–3	1	1	1.5636	1.5635	0.0001
0	6	0	1.5550	1.5550	0.0000
–2	4	1	1.5535	1.5536	–0.0001
2	2	1	1.5446	1.5447	–0.0001

Unit Cell Par. (obs)	Unit Cell Par.[160]
a = 9.8818 Å	a = 9.9 Å
b = 18.0227 Å	b = 18.0 Å
c = 5.3123 Å	c = 5.3 Å
β = 103.73º	β = 104.0º
V = 919.089 Å^3	V = 916.41 Å^3; Z = 2
	Monoclinic ($C2/m$)

the X-ray powder diagrams for each mineral (given in Tables 10–13) were used to determine the unit cell parameters of the studied samples. It was found that they are in a very good agreement with the corresponding literature data.[157–160]

CONCLUSION

The strong and broad bands in the FT-Raman spectrum of almandine observed at 446 and 607 cm^{-1} are found to be fluorescence bands that appear from the traces of rare earth impurities. Therefore, the Raman studies of the minerals, when using FT technique, should be additionally extended in the Anti-Stokes side of the spectra.

The intensity and especially the frequency of the IR band in the ν(OH) region serve as a tool for reliable determination of the presence of Fe^{3+} and/or Al^{3+} in epidote and discriminate between epidote and clinozoisite. Despite the expressed IR spectral similarity between the studied sorosilicates, their Raman spectra exhibit considerable differences confirming that they are sensitive to the compositional changes and the structural disorder appearance. In the case of amphiboles, the intensity and especially the number of the IR bands in the ν(OH) region could serve for exact mineral identification. It is based on the presence of different Y cations in M1 and M3 octahedral sites which is manifested by different spectral view.

Although the centre of inversion is present in the space groups of the studied clinoamphiboles and pyroxenes, the IR-Raman doublets were observed. Their appearance is due to the presence of *TOT* strips in the structures whose stacking sequence symmetry dominates over the crystal symmetry and determines the activity of the normal modes. The higher wavenumber of the characteristic $\nu(XO_6)$ modes in the IR spectra of the pyroxenes compared to the lower wavenumbers of the corresponding mode in the spectra of pyroxenoids could be used to discriminate between pyroxenes and pyroxenoids. Furthermore, the number of the IR bands in the 800–650 cm^{-1} region could serve as an indication about the number of the tetrahedra in its repeating unit.

Variation of the degree of the sensitivity to impurities between both vibrational techniques justifies their simultaneous application confirming that they are complementary techniques. Namely, both techniques could distinguish between the isomorphous mineral types.

The X-ray powder diffraction technique enables a rapid check of the studed silicate mineral authencity, giving an unambiguous opportunity for their characterization. In addition, some identification difficulties that might arise from the low quality vibrational spectra are overcome by the investigation of the X-ray powder diffraction diagrams. Although both techniques are complementary rather than competitive, the analysis of the silicate minerals proves that the X-ray powder diffraction is more sensitive to mineral impurities determination compared to the vibrational spectroscopy.

Acknowledgement. The financial support from the Ministry of Education and Science of the Republic of Macedonia is gratefully acknowledged.

REFERENCES

1. M. Trajkovska, B. Šoptrajanov, G. Jovanovski, and T. Stafilov, *J. Mol. Struct.* **267** (1992) 191–196.
2. M. Trajkovska, B. Šoptrajanov, T. Stafilov, and G. Jovanovski, *Geol. Macedonica* **7** (1993) 55–59.
3. B. Šoptrajanov, M. Trajkovska, I. Gržetić, G. Jovanovski, and T. Stafilov, *N. Jb. Miner. Abh*. **166** (1993) 83–89.
4. B. Šoptrajanov, M. Trajkovska, G. Jovanovski, and T. Stafilov, *N. Jb. Miner. Abh.* **167** (1994) 329–337.
5. B. Šoptrajanov, M.Trajkovska, T. Stafilov, G. Jovanovski, and I. Gržetić, *Spectrosc. Lett*. **30** (1997) 79–87.

6. G. Jovanovski, V. Stefov, B. Jovanovski, B. Šoptrajanov, and B. Kaitner, *16th Congress of Chemists and Technologists of Macedonia, Book of Papers,* Skopje, 1999, 43–46.
7. V. Stefov, S. Dimitrovska, G. Jovanovski, and B. Šoptrajanov, *16th Congress of Chemists and Technologists of Macedonia, Book of Papers,* Skopje, 1999, 47–50.
8. G. Jovanovski, V. Stefov, B. Jovanovski, B. Šoptrajanov, and B. Boev, *Geol. Macedonica* **13** (1999) 69–74.
9. V. Stefov, G. Jovanovski, B. Šoptrajanov, B. Minčeva-Šukarova, S. Dimitrovska, and B. Boev, *Geol. Macedonica* **14** (2000) 61–66.
10. P. Makreski, G. Jovanovski, V. Stefov, B. Minčeva-Šukarova, B. Kaitner, and B. Boev, *Geol. Macedonica* **15–16** (2001–2002) 43–50.
11. B. Boev, V. Bermanec, T. Serafimovski, S. Lepitkova, S. Mikulčić, M. Šoufek, G. Jovanovski, T. Stafilov, and M. Najdoski, *Geol. Macedonica* **15** (2001) 1–23.
12. G. Jovanovski, B. Minčeva-Šukarova, P. Makreski, B. Šoptrajanov, W. P. Griffith, and R. L. Willis, *Eighteenth International Conference on Raman Spectroscopy*, *Proceedings*, Budapest, 2002, 931–932.
13. G. Jovanovski, B. Minčeva-Šukarova, P. Makreski, V. Stefov, W. P. Griffith, and R. L. Willis, *Eighteenth International Conference on Raman Spectroscopy*, *Proceedings*, Budapest, 2002, 933–934.
14. G. Jovanovski, V. Stefov, B. Šoptrajanov, and B. Boev, *N. Jb. Miner. Abh.* **177** (2002) 241–253.
15. B. Minčeva-Šukarova, G. Jovanovski, P. Makreski, B. Soptrajanov, W. P. Griffith, R. L. Willis, and I. Grzetic, *J. Mol. Struct.* **651–653** (2003) 181–189.
16. P. Makreski and G. Jovanovski, *Bull. Chem. Technol. Macedonia* **22** (2003) 25–32.
17. G. Jovanovski, B. Boev, P. Makreski, M. Najdoski, and G. Mladenovski, *Bull. Chem. Technol. Macedonia* **22** (2003) 111–141.
18. P. Makreski, G. Jovanovski, B. Minčeva-Šukarova, B. Soptrajanov, A. Green, B. Engelen, and I. Gržetic, *Vib. Spectrosc.* **35** (2004) 59–65.
19. P. Makreski, G. Jovanovski, B. Kaitner, T. Stafilov, B. Boev, and D. Cibrev, *N. Jb. Miner. Abh.* **180** (2004) 215–243.
20. P. Makreski, G. Jovanovski, T. Stafilov, and B. Boev, *Bull. Chem. Technol. Macedonia* **23** (2004) 171–184.
21. P. Makreski, G. Jovanovski, and S. Stojančeska, *J. Mol. Struct.* **744–747** (2005) 79–92.
22. P. Makreski, G. Jovanovski, and S. Dimitrovska, *Vib. Spectrosc.* **39** (2005) 229–239.
23. B. Boev, G. Jovanovski, P. Makreski, and V. Bermanec, *Geol. Macedonica* **19** (2005) 39–56.
24. G. Jovanovski, P. Makreski, B. Šoptrajanov, B. Kaitner, and B. Boev, *Contributions, Sec. Math. Tech. Sci., MANU* **26** (2005) 7–84.
25. P. Makreski, G. Jovanovski, A. Gajović, T. Biljan, D. Angelovski, and R. Jaćimović, *J. Mol. Struct.* **788** (2006) 102–114.
26. P. Makreski, G. Jovanovski, and A. Gajović, *Vib. Spectrosc.* **40** (2006) 98–109.
27. P. Makreski, G. Jovanovski, B. Kaitner, A. Gajović, and T. Biljan, *Vib. Spectrosc.* **44** (2007) 162–170.
28. V. Šontevska, G. Jovanovski, and P. Makreski, *J. Mol. Struct.* **834–836** (2007) 318–327.
29. P. Makreski and G. Jovanovski, *J. Raman Spectrosc.* **39** (2008) 1210–1213.
30. V. Šontevska, G. Jovanovski, P. Makreski, A. Raškovska, and B. Šoptrajanov, *Acta Chim. Slov.* **55** (2008) 757–766.
31. T. Stafilov, V. Jordanovska, and S. Aleksovska, *Bull. Chem. Technol. Macedonia* **8** (1990) 93–98.
32. T. Stafilov, V. Jordanovska, and S. Aleksovska, *Vest. Slov. Kem. Drus.* **37** (1990) 141–148.
33. T. Stafilov, V. Jordanovska, and S. Aleksovska, *Bull. Chem. Technol. Macedonia* **9** (1990) 159–166.
34. T. Stafilov, A. Lazaru, and E. Pernicka, *Acta Chim. Slov.* **40** (1993) 37–46.
35. A. Lazaru and T. Stafilov, *Geol. Macedonica* **7** (1993) 73–80.
36. T. Balić Žunić, T. Stafilov, and D. Tibljaš, *Geol. Macedonica* **7** (1993) 45–52.
37. T. Stafilov, A. Lazaru, and E. Pernicka, At. Spectrosc. **16** (1995) 158–161.
38. T. Stafilov and A. Lazaru, *Geol. Macedonica* **10** (1996) 83–86.
39. A. Lazaru and T. Stafilov, *Anal. Lab.* **6** (1997) 101–103.
40. A. Lazaru, and T. Stafilov, *Fresenius' J. Anal. Chem.* **360** (1998) 726–728.
41. A. Lazaru, R. Ilić, J. Skvarč, E. S. Krištof, and T. Stafilov, *Radiat. Meas.* **31** (1999) 677–682.
42. T. Stafilov, *Spectrochim. Acta, Part B* **55** (2000) 893–906.
43. D. Zendelovska, T. Stafilov, and B. Boev, *Geol. Macedonica* **14** (2000) 67–73.
44. A. Lazaru and T. Stafilov, *Bull. Chem. Technol. Macedonia* **19** (2000) 21–26.
45. T. Stafilov and D. Zendelovska, *Acta Chim. Slov.* **47** (2000) 81–88.
46. D. Zendelovska and T. Stafilov, *Anal. Sci.* **17** (2001) 425–428.
47. D. Zendelovska, G. Pavlovska, K. Čundeva, and T. Stafilov, *Talanta* **54** (2001) 139–146.
48. T. Stafilov and D. Zendelovska, *Turk. J. Chem.* **26** (2002) 271–280.
49. A. Lazaru, R. Jaćimović, R. Ilić, D. Mihajlović, and T. Stafilov, *J. Radioanal. Nucl. Chem.* **253** (2002) 427–434.
50. T. Stafilov, D. Zendelovska, G. Pavlovska, and K. Čundeva, *Spectrochim. Acta, Part B* **57** (2002) 907–917.
51. P. Makreski, V. Paneva, G. Jovanovski, T. Stafilov, and D. Zendelovska, *3rd Aegean Analytical Chemistry Days*, *Proceedings*, Polihnotos, Lezvos, (2002) 440–443.
52. K. Čundeva, T. Stafilov, D. Zendelovska, and G. Pavlovska, *Bull. Chem. Technol. Macedonia* **21** (2002) 43–52.
53. K. Čundeva, G. Pavlovska, T. Stafilov, and D. Zendelovska, *J. Inst. Sci. Techn. Balikesir Univ.* **4** (2002) 9–12.
54. N. Angelov and T. Stafilov, *Geol. Macedonica* **17** (2003) 73–82.
55. V. Zajkova, T. Stafilov, and B. Boev, *Geol. Macedonica* **17** (2003) 87–93.
56. G. Pavlovska, K. Čundeva, T. Stafilov, and D. Zendelovska, *Sep. Sci. Technol.* **38** (2003) 1117–1124.
57. T. Stafilov, N. Angelov, R. Jaćimović, and V. Stibilj, *Microchim. Acta* **149** (2005) 229–237.
58. V. Zajkova Paneva, K. Čundeva, and T. Stafilov, *Spectrochim. Acta, Part B* **60** (2005) 403–407.
59. M. Taseska, T. Stafilov, P. Makreski, and G. Jovanovski, *Ovidius University*, *Ann. Chem.* **16** (2005) 43–46.
60. R. Jaćimović, P. Makreski, V. Stibilj, T. Stafilov, and G. Jovanovski, *Geol. Macedonica* **19** (2005) 33–38.
61. M. Taseska, T. Stafilov, P. Makreski, R. Jaćimović, V. Stibilj, and G. Jovanovski, *Geol. Macedonica* **20** (2006) 33–38.
62. V. Zajkova Paneva, K. Čundeva, and T. Stafilov, *Geostand. Geoanal. Res.* **31** (2007) 51–60.
63. R. Jaćimović, M. Taseska, V. Stibilj, P. Makreski, T. Stafilov, and G. Jovanovski, *Geol. Macedonica* **21** (2007) 87–91.
64. D. Bish and J. Post, *Am. Mineral.* **78** (1993) 932–940.
65. E. Libowitzky, *Croat. Chem. Acta* **79** (2006) 299–309.
66. D. Yu. Pushcharovsky, *Croat. Chem. Acta* **73** (2000) 869–886.
67. V. C. Farmer (Ed.), *The Infrared Spectra of Minerals*, Mineralogical Society, London, 1974.
68. P. F. McMillan and A. M. Hofmeister, *Rev. Mineral.* **18** (1988) 99–157.
69. W. P. Griffith, *Raman Spectroscopy of Minerals*, in: V. C. Farmer (Ed.), *The Infrared Spectra of Minerals*, Mineralogical Society, London, 1974, pp. 119–135.

70. L. Burgio and R. J. H. Clark, *Spectrochim. Acta, Part A* **57** (2001) 1491–1521.
71. A. E. Milodowski and D. J. Morgan, *Nature* **286** (1980) 248–248.
72. S. J. Gaffey, *Am. Mineral.* **71** (1986) 151–162.
73. R. Shirley , *The CRYSFIRE System for Automatic Powder Indexing*. (http://www.ccp14.ac.uk/tutorial/crys/).
74. J. Laugier and B. Bochu, *LMGP-Suite Suite of Programs for the interpretation of X-ray Experiments*, ENSP/Laboratoire des Matériaux et du Génie Physique, BP 46. 38042 Saint Martin d'Hères, France. (http://www.inpg.fr/LMGP and http://www.ccp14.ac.uk/tutorial/lmgp/).
75. GRAMS32 for Microsoft Windows, Vers. 4.10, Galactic Industries Corporation, 1991–1996.
76. M. Arsovski and N. Dumurdžanov, *Geol. Macedonica* **9** (1995) 15–22.
77. W. D. Nesse, *Introduction to Mineralogy*, Oxford University Press, New York, 2000.
78. F. Liebau, *Structural Chemistry of Silicates*, Springer-Verlag, New York, 1985.
79. http://www.geo.vu.nl/users/ima-cnmmn/
80. http://www.webmineral.com/
81. *Inorganic Library of FT IR Spectra – Minerals*, NICODOM, 1998.
82. T. Boffa Ballaran, M. A. Carpenter, G. A. Geiger, and A. M. Koziol, *Phys. Chem. Miner.* **26** (1999) 554–569.
83. H. Moenke, *Mineralspektren*, Vol. I, Academie, Berlin, 1962.
84. R. K. Moore, W. B. White, and T. V. *Long, Am. Mineral.* **56** (1971) 54–71.
85. A. M. Hofmeister and A. Chopelas, *Phys. Chem. Miner.* **17** (1991) 503–526.
86. P. Dawson, M. M. Hargreave, and G. R. Wilkinson, *J. Phys. C* **4** (1971) 240–256.
87. R. Hubin and P. Tarte, *Spectrochim. Acta*, *Part A* **27** (1971) 683–690.
88. G. R. Rossman, *Trans. Am. Crystallogr. Assoc.* **15** (1979) 107–120.
89. P. Tarte, *Spectrochim. Acta* **19** (1963) 25–47.
90. R. G. Burns and F. E. Huggins, *Am. Mineral.* **57** (1972) 967–985.
91. A. Beran, K. Langer, and M. Andrut, *Mineral. Petrol.* **48** (1993) 257–268.
92. P. Tarte, *Bull. Soc. Fr. Ceram.* **58** (1963) 13–34.
93. M. Koch-Müller, K. Langer, and A. Beran, *Phys. Chem. Miner.* **22** (1995) 108–114.
94. W. P. Griffith, *J. Chem. Soc. A* (1969) 1372–1377.
95. B. A. Kolesov and C. A. Geiger, *J. Raman Spectrosc.* **28** (1997) 659–662.
96. B. A. Kolesov and C. A. Geiger, *Phys. Chem. Miner.* **25** (1998) 142–151.
97. T. Calligaro, S. Colinart, J. P. Poirot, and C. Sudres, *Nucl. Instrum. Methods Phys. Res., Sect B* **189** (2002) 320–327.
98. E. Salje, C. Schmidt, and U. Bismayer, *Phys. Chem. Miner.* **19** (1993) 502–506.
99. F. Guyot, H. Boyer, M. Madon, B. Velde, and J. P. Poirier, *Phys. Chem. Miner.* **13** (1986) 91–95.
100. T. P. Mernagh and L. Liu, *Phys. Chem. Miner*. **18** (1991) 126–130.
101. Powder Diffraction File-4/Minerals, International Center for Diffraction Data, Pennsylvania, 2005.
102. T. Armbruster, C. A. Geiger, and G. A. Lager, *Am. Mineral.* **77** (1992) 512–521.
103. G. A. Novak and G. V. Gibbs, *Am. Mineral.* **56** (1971) 791–825.
104. G. Jovanovski, B. Kaitner, P. Makreski, B. Boev, and S. Stojančevska, *14th Croatian-Slovenian Crystallographic Meeting*, *Book of Abstracts*, Vrsar, 2005, p. 38.
105. K. Langer and M. Raith, *Am. Mineral.* **59** (1974) 1249–1258.
106. A. Liebscher, *Rev. Mineral. Geochem.* **56** (2004) 125–170.
107. G. Della Ventura, A. Mottana, G. C. Parodi, and W. L. Griffith, *Eur. J. Mineral.* **8** (1996) 655–665.
108. A. N. Lazarev, *Kristallografiya* **6** (1961) 125–127.
109. E. Libowitzky and G. R. Rossman, *Eur. J. Mineral.* **9** (1997) 793–802.
110. P. H. Poulet and J. P. Mathieu, *Bull. Soc. Fr. Mineral. Cristallogr.* **98** (1975) 3–5.
111. R. Brunel and R. Vierne, *Bull. Soc. Fr. Mineral. Cristallogr.* **100** (1977) 14–20.
112. B. Güttler, E. Salje, and S. Ghose, *Phys. Chem. Miner.* **16** (1989) 606–613.
113. A. Wang, J. Han, L. Guo, J. Yu, and P. Zeng, *Appl. Spectrosc.* **48** (1994) 959–968.
114. Raman Spectra Database of Minerals and Inorganic Materials posted by National Institute of Advanced Industrial and Science Technology (http://www.aist.go.jp/RIODB/rasmin/E_index.htm).
115. Raman Spectra of Minerals collected at the Physics Department of the Univesrsity of Parma (http://www.fis.unipr.it./~bersani/raman/raman/spettri.htm).
116. S. E. Bradbury and Q. Williams, *Am. Mineral.* **88** (2003) 1460–1470.
117. S. V. Gavorkyan, *Mineral. Z.* **12** (1990) 63–66.
118. S. Petrusenko, M. N. Taran, A. N. Platonov, and S. V. Gavorkyan, *Rev. Bulgarian Geol. Soc.* **53** (1992) 1–9.
119. S. Heuss-Aβbichler, *Habilitationthesis*, München, 2000, p. 105.
120. J. H. Denning, R. F. Hudson, D. R. Laughlin, and S. D. Ross, *Spectrochim. Acta, Part A* **28** (1972) 1787–1791.
121. A. N. Lazarev, *Vibrational Spectra and Structure of Silicates*, Plenum, New York, 1972.
122. J. J. Papike, *Am. Mineral.* **81** (1996) 525–544.
123. H. Y. McSween, Jr., *Meteoritics* **29** (1994) 757–779.
124. A. Wang, B. L. Jolliff, L. A. Haskin, K. E. Kuebler, and K. M. Viskupic, *Am. Mineral.* **86** (2001) 790–806.
125. M. Cameron, S. Sueno, C. T. Prewitt, and J. J. Papike, *Am. Mineral.* **58** (1973) 594–618.
126. R. L. Freed and D. R. Peacor, *Am. Mineral.* **52** (1967) 709–720.
127. S. Ghose, P. K. Sen Gupta, R. C. Boggs, and E. O. Schlemper, *Am. Mineral.* **74** (1989) 1084–1090.
128. W. V. Maresch and A. Mottana, *Contrib. Mineral. Petrol.* **55** (1976) 69–79.
129. Y. Ohashi and L. W. Finger, *Am. Mineral.* **63** (1978) 274–288.
130. R. Jaćimović, B. Smodiš, T. Bučar, and P. Stegnar, *J. Radioanal. Nucl. Chem.* **257** (2003) 659–663.
131. F. De Corte, R. Van Sluijs, A. Simonits, J. Kučera, B. Smodiš, A.R. Byrne, A. De Wispelaere, D. Bossus, J. Frána, Z. Horák, and R. Jaćimović, *Fresenius' J. Anal. Chem.* **370** (2001) 38–41.
132. M. V. Zeller and M. P. Juszli, *Reference Spectra of Minerals*, Perkin-Elmer Corporation, 1975, p. 30.
133. M. S. Rutstein and W. B. White, *Am. Mineral.* **56** (1971) 877–887.
134. P. R. Christensen, J. L. Bandfield, V. E. Hamilton, D. A. Howard, M. D. Lanr, J. L. Piatek, S. W. Ruff, and W. L. Stafanov, *J. Geophys. Res.* **105** (2000) 9735–9739.
135. R. G. J. Sterns, *The common chain, ribbon, and ring silicates*, in: V. C. Farmer (Ed.), *Infrared Spectra of Minerals*, Mineralogical Society, London, UK, 1974, p. 305.
136. K. Viswanathan, *Am. Mineral.* **66** (1981) 1080–1085.
137. M. Schmidt and H. D. Lutz, *Phys. Chem. Miner.* **20** (1993) 27–32.
138. E. Huang, C. H. Chen, T. Huang, E. H. Lin, and J.-A. Xu, *Am. Mineral.* **85** (2000) 473–479.
139. G. A. Hope, R. Woods, and C. G. Munce, *Miner. Eng*. **14** (2001) 1565–1577.
140. S. J. Mills, R. L. Frost, J. T. Kloprogge, and M. L. Weier, *Spectrochim. Acta, Part A* **62** (2005) 171–175.
141. T. P. Mernagh and D. M. Hoatson, *J. Raman Spectrosc.* **28**

(1997) 647–658.
142. M. S. Bilton, T. R. Gilson, and M. Webster, *Spectrochim. Acta, Part A* **28** (1972) 2113–2119.
143. W. G. Ernst and C. M. Wai, *Am. Mineral.* **55** (1970) 1226–1258.
144. Ph. Gillet, B. Reynard, and C. Tequi, *Phys. Chem. Miner.* **16** (1989) 659–667.
145. R. G. Burns and R. G. J. Streens, *Science* **155** (1966) 890–892.
146. N. O. Gopal, K. V. Narasimhulu, and J. L. Rao, *Spectrochim. Acta* **60** (2004) 2441–2448.
147. K. Ishida, F. C. Hawthorne, and Y. Ando, *Am. Mineral.* **87** (2002) 891–898.
148. R. W. T. Wilkins, *Am. Mineral.* **55** (1970) 1993–1998.
149. H. F. Shurvell, L. Rintoul, and P.M. Fredericks, *Int. J. Vibr. Spec.* [www.ijvs.com] **5** (2001) 5, 4.
150. D. G. Taylor, C. M. Nenadic, and J. V. Crable, *Am. Ind. Hyg. Assoc. J.* **31** (1970) 100–108.
151. R. G. Burns and C. Greaves, *Am. Mineral.* **56** (1971) 2010–2033.
152. K. Ishida and F. C. Hawthorne, *Am. Mineral.* **86** (2001) 965–972.
153. A. N. Buckley and R. W. T. Wilkins, *Am. Mineral.* **56** (1971) 90–100.
154. R. W. T. Wilkins, L. R. Davidson, and J. R. Ross, *Contrib. Mineral. Petrol.* **28** (1970) 280–287.
155. D. Slovenec and V. Bermanec, *Systematic Mineralogy – Mineralogy of the Silicates*, Denona d.o.o., Zagreb, 2003, pp. 145–177.
156. http://minerals.gps.caltech.edu/files/raman
157. J. J. Papike and M. Ross, *Am. Mineral.* **53** (1968) 1156–1173.
158. R. Oberti, L. Ungaretti, E. Cannillo, F. C. Hawthorne, and I. Memmi, *Eur. J. Miner.* **7** (1995) 1049–1063.
159. B. W. Evans and H. Yang, *Am. Mineral.* **83** (1998) 458–475.
160. F. C. Hawthorne, *Can. Mineral.* **14** (1976) 346–356.

SAŽETAK

Silikatni minerali iz Makedonije. Komplementarno korištenje vibracijske spektroskopije i rentgenske difrakcije na polikristalu u svrhu prepoznavanja i otkrivanja

Gligor Jovanovski,[a,b] Petre Makreski,[a] Branko Kaitner[c] i Blažo Boev[d]

[a]*Institute of Chemistry, Faculty of Science, SS. Cyril and Methodius University, P.O. Box 162, MK-1001 Skopje, Republic of Macedonia*
[b]*Macedonian Academy of Sciences and Arts, P.O. Box 428, MK-1001 Skopje, Republic of Macedonia*
[c]*Department of Chemistry, Faculty of Science, University of Zagreb, Horvatovac 102a, 10000 Zagreb, Croatia*
[d]*Faculty of Mining, Geology and Polytechnic, Goce Delčev University, Krste Misirkov bb, P.O. Box 201, MK-2000 Štip, Republic of Macedonia*

Ovaj pregledni rad predstavlja rezultate komplementarne uporabe vibracijske spektroskopije (infracrvene i ramanske) i rentgenske difrakcije na polikristalu u svrhu otkrivanja i prepoznavanja makedonskih silikatnih minerala.